

**NASA
SPACE VEHICLE
DESIGN CRITERIA
(ENVIRONMENT)**

NASA SP-8118

**INTERPLANETARY
CHARGED PARTICLE
MODELS (1974)**



MARCH 1975

NATIONAL AERONAUTICS AND SPACE ADMINISTRATION

FOREWORD

NASA experience has indicated a need for uniform criteria for the design of space vehicles. Accordingly, criteria have been developed in the following areas of technology:

Environment
Structures
Guidance and Control
Chemical Propulsion

Individual components of this work are issued as separate monographs as soon as they are completed. A list of the titles that have been published to date can be found at the end of this monograph.

These monographs are to be regarded as guides to design and not as NASA requirements except as may be specified in formal project specifications. It is expected, however, that the monographs will be used to develop requirements for specific projects and be cited as the applicable documents in mission studies or in contracts for the design and development of space vehicle systems.

This monograph was prepared under the cognizance of the Goddard Space Flight Center with Scott A. Mills as program coordinator. The principal author was Neil Divine of the Jet Propulsion Laboratory. Valuable contributions were also made by A. J. Beck, F. D. Palluconi, and D. M. Wexler of the Jet Propulsion Laboratory, and by J. H. King of Goddard Space Flight Center.

Comments concerning the technical content of these monographs will be welcomed by the National Aeronautics and Space Administration, Goddard Space Flight Center, Systems Reliability Directorate, Greenbelt, Maryland 20771.

March 1975

For sale by the National Technical Information Service
Springfield, Virginia 22151
Price -- \$3.75

CONTENTS

1. INTRODUCTION	1
2. STATE OF THE ART	1
2.1 Solar Wind	2
2.1.1 Theory	2
2.1.2 Indirect Observations	3
2.1.3 Spacecraft Observations	4
2.1.3.1 Proton Properties	4
2.1.3.2 Heavier Ions	5
2.1.3.3 Electrons	6
2.1.3.4 Magnetic Fields	6
2.1.4 Dynamics	6
2.1.5 Position Dependences	8
2.2 Galactic Cosmic Rays	9
2.2.1 Observations	9
2.2.2 Theory	10
2.2.3 Numerical Representations	12
2.2.4 Time and Position Dependences	15
2.3 Solar Particle Events	16
2.3.1 Observations	16
2.3.2 Theory	16
2.3.3 Data Availability	17
2.3.4 Application of Data to Mission Planning	18
2.3.5 Long-Term Probabilities for Peak Intensities and Fluences	19
2.3.6 Other Energies and Particles	25
3. CRITERIA	26
3.1 Solar Wind	27
3.2 Galactic Cosmic Rays	28
3.2.1 Electron Component	30
3.2.2 Proton Component	30
3.2.3 Other Nuclei	31
3.3 Solar Particle Events	31
3.3.1 Peak Proton Intensity	32
3.3.2 Proton Fluence	32
3.3.3 Other Particles and Energies	32

REFERENCES 34

APPENDIX A. Symbols 38

APPENDIX B. Glossary 40

NASA SPACE VEHICLE DESIGN CRITERIA MONOGRAPHS 41

INTERPLANETARY CHARGED PARTICLE MODELS (1974)

1. INTRODUCTION

The design of space vehicles for operation in interplanetary space requires both qualitative and quantitative descriptions of charged particle environments. These environments comprise the solar wind, solar particle events, and galactic cosmic rays, for all of which extensive data have been reported in the literature. The state-of-the-art review and the resulting design criteria that are developed in the following sections are based primarily on findings of experiments aboard interplanetary and high-altitude earth-orbiting spacecraft.

The charged particles of interplanetary space require serious design consideration because of a number of observed effects on space vehicles. Solar cells are particularly sensitive to charged particle impact; important degradation in their power output has been traced to the effect of prolonged exposure to the solar wind. Solar protons may similarly impact the reliability of electric propulsion systems. Degradation of other spacecraft surfaces, particularly coatings and lenses, sometimes occurs after long exposure to interplanetary space. Energetic proton impact occasionally causes interference, detector saturation, or spurious signals in experiments and spacecraft subsystems during severe solar particle events. Galactic cosmic ray impact can lead to interference and failure in sensitive (shielded and unshielded) electronic components and subsystems as well as to registering in solid state and other detectors, photographic films, and other emulsions. Because of the importance of these spacecraft responses for long-term interplanetary and planetary missions, thorough descriptions of charged particle intensity, their fluence and their variations with time, position, and particle kind and energy are needed.

Charging of spacecraft by energetic particles is also of concern. The design review team for the Helios project concluded that solar wind electron measurements might be affected because of differential charging when shadowed portions of the spacecraft acquired a negative charge from electron impact. Accordingly, steps were taken to avoid this possibility. For spacecraft charging, NASA SP-8111 (Assessment and Control of Electrostatic Charges) should be used in conjunction with the data of this monograph.

The environmental descriptions provided in this monograph apply to interplanetary space between 0.1 and 10 AU from the Sun except within the magnetospheres of the Earth and other planets with magnetic fields. The criteria developed herein complement space vehicle design criteria for the related environments of solar electromagnetic radiation and trapped radiation belts of Earth, Jupiter, Saturn, Uranus, and Neptune, which have been published and are listed at the end of this monograph.

2. STATE OF THE ART

The environment of interplanetary charged particles has three components, two steady and one sporadic: the solar wind, galactic cosmic rays, and solar particle events. The following

sections review state-of-the-art knowledge of these components. The appendices provide definitions of symbols and a glossary.

2.1 Solar Wind

The solar wind is a fully-ionized plasma that steadily streams outward from the Sun in all directions in approximately radial paths. The mass and energy flux are dominated by the proton component, for which typical densities and flow speeds near the Earth's orbit are 5 cm^{-3} and 400 km/s for a proton energy near 1 keV . Heavier nuclei, electrons, and the interplanetary magnetic field participate in the flow which has characteristics that vary with time and space. The flow represents a very minor contribution to the overall budget of the Sun: mass loss annually to the solar wind is about 10^{14} times the Sun's mass, and the power of kinetic energy in solar wind is between 10^7 and 10^6 times the power radiated as sunlight.

2.1.1 Theory

Before in-situ interplanetary observations, some of the important properties of the solar wind were predicted on the basis of theoretical considerations and indirect observations (sec. 2.1.2). The theories, introduced by Parker (ref. 1) and refined since by many others (reviewed in ref. 2), are based on the origin of the solar wind in the Sun's chromosphere where ionization and heating occur by acoustic or magnetic noise coupled to turbulence in the underlying photosphere. Because back-pressure from the interplanetary medium is negligible, the hot plasma expands radially. This phenomenon is manifested first as the corona and then (beyond some ten solar radii) as a supersonic expansion (relative to the speeds of acoustic and Alfvén waves). The expansion is accelerated by the Sun's spherical divergence and gravity in a manner analogous to that which governs exhaust flow through a nozzle.

Theoretical solutions of the hydrodynamic equations that describe such a flow (using conditions near the Sun as input data) predict average values for the density, velocity, and temperature of the plasma near the Earth's orbit that are close to observed values. Confidence is thus established in the predicted radial dependences of these quantities (sec. 2.1.5). At large distances from the Sun the solar wind presumably terminates by interacting with the interstellar medium (relatively cold, non-ionized gas), but the location of the heliosphere's boundary is not well determined either from theory (sample recent analyses are provided by references 3 and 4) or from observations although a lower limit of 3.5 AU exists (sec. 2.1.2). For present purposes a conservative approach is adopted that ignores this boundary and assumes extension of the solar wind to infinity.

Calculated recombination lifetimes are so much larger than flow times out to several AU from the Sun that the solar wind plasma remains effectively fully-ionized throughout interplanetary space. This plasma behaves in many respects as a fluid and transports

magnetic fields from regions near the solar surface radially into interplanetary space. The combination of this transport and solar rotation leads to an interplanetary configuration of magnetic field lines (each resembling an Archimedes spiral). The field lines form an even number of sectors that rotate with the Sun with alternate sectors having the same polarity (the magnetic field within a rotating sector is directed approximately inward or outward along the spiral on the average). As modified by solar wind streaming (sec. 2.1.4), this general structure is verified by spacecraft magnetometer observations (sec. 2.1.3.4).

2.1.2 Indirect Observations

From dynamic interactions of the solar wind with type I (ion) tails of comets, the solar wind's pressure has been inferred at distances up to a few AU from the Earth in directions not confined to the ecliptic plane. Quantitatively, however, the evidence for solar wind properties is partially obscured by the individual characteristics, time variability, and selection effects of the comets in the observed samples. The major pertinent conclusions from such analyses, abstracted from references 5 and 6, are (a) the solar wind radiates in all directions to at least 3.5 AU from the Sun, (b) its properties vary somewhat with ecliptic latitude, and (c) its velocity, which correlates with indices of geomagnetic activity, e.g., ΣK_p , always exceeds 150 km/s with a mean radial component of 500 km/s and an azimuthal component of 5 to 10 km/s that moves in the direction of solar rotation.

Complementary to comet-tail observations that yield information on the massive, proton component of the solar wind, observations of the scintillation (at 0.1 to 10 Hz) of small diameter radio sources (ref. 7) have been interpreted as fluctuations, on a scale near 100 km, in the electron density of $(0.14 \text{ cm}^{-2})S^{-2}$ for the region $0.2 < S < 0.9$ AU from the Sun. These conclusions are supported, with a modestly different dependence on S , by the scintillation discussion in reference 8.

Additional indirect information on solar wind properties can be inferred (ref. 6) from the time delay between observation of flares on the solar surface and associated geomagnetic disturbances (sudden commencements) that yield average velocities for shock front propagation; from various aspects of geomagnetic disturbances that yield solar wind variability information; from the polarization of zodiacal light that yields electron density; from the green coronal emission lines that yield plasma emissivity and temperature near the Sun; from solar Lyman- α radiation scattered by neutral hydrogen that yields some interaction characteristics between the plasma densities and the neutral gas; from dynamic spectra of solar radio bursts that yield plasma densities and temperatures near the Sun; from scattering of extended radio source emission that yields electron densities and plasma filamentary structure; from ground-based radar and satellite radio transmissions that yield electron density and its fluctuations; and from cosmic ray variations that yield information on solar wind-carried magnetic field fluctuations. Most of the inferences are not discussed here because they are consistent with the results of spacecraft observations which provide more detail and reliability for the quantities involved.

2.1.3 Spacecraft Observations

Numerous spacecraft-borne instruments, particularly Faraday cups, electrostatic analyzers, charged particle telescopes, and search coil and flux gate magnetometers, perform in-situ measurements of solar wind properties in interplanetary space beyond the Earth's magnetosphere. The following spacecraft carry these instruments: Earth-orbiting satellites with apogee distances greater than about 60,000 km (ten Earth radii), notably members of the IMP (Explorer) and Vela series, HEOS 1, and OGO 5; lunar orbiters and landers, notably Explorer 35; and planetary and interplanetary vehicles, notably members of the Pioneer and Mariner series.

Characteristics of the solar wind that have been derived from data taken near the Earth's orbit are given in the following sections.

2.1.3.1 Proton Properties

Figure 1 (adapted from references 9 and 10) includes sample histograms of proton concentrations, flow speed, flow direction, and temperature. In each case the most

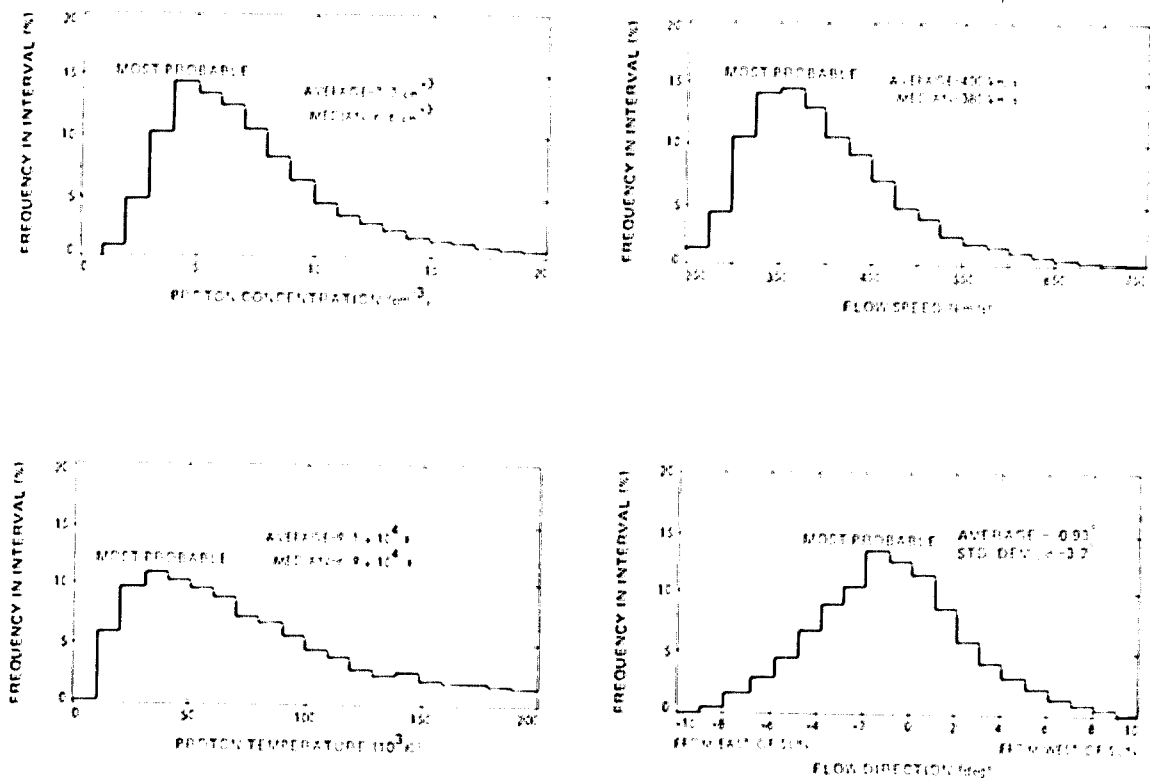


Figure 1.—Sample distributions of proton characteristics in the solar wind near 1 AU. Data measured in 1965-1967 by the electrostatic analyzer systems on the Vela 3 (A and B) satellites (refs. 9 and 10).

probable, median, and mean values increase in that order. To within about a factor 2 (typical of the upper limit for differences among various experiments), representative average proton values are 5 cm^{-3} for the concentration, 425 kms^{-1} for the flow speed, 1 degree prograde for the angular departure from the radial, and $8 \times 10^4 \text{ K}$ for the temperature. Additional details in the distributions, particularly the slight proton temperature anisotropy are of considerable scientific interest, but are ignored here because they are insignificant compared to the large variability in the foregoing average quantities. Typical ranges and extremes* of selected quantities, derived from published histograms and other sources are adopted for design criteria (sec. 3.1).

2.1.3.2 Heavier Ions

Figure 2 (from refs. 11 and 12) is representative of composition measurements (reviewed in ref. 12) and shows that ions heavier than He^{++} are present in the solar wind. As such ions

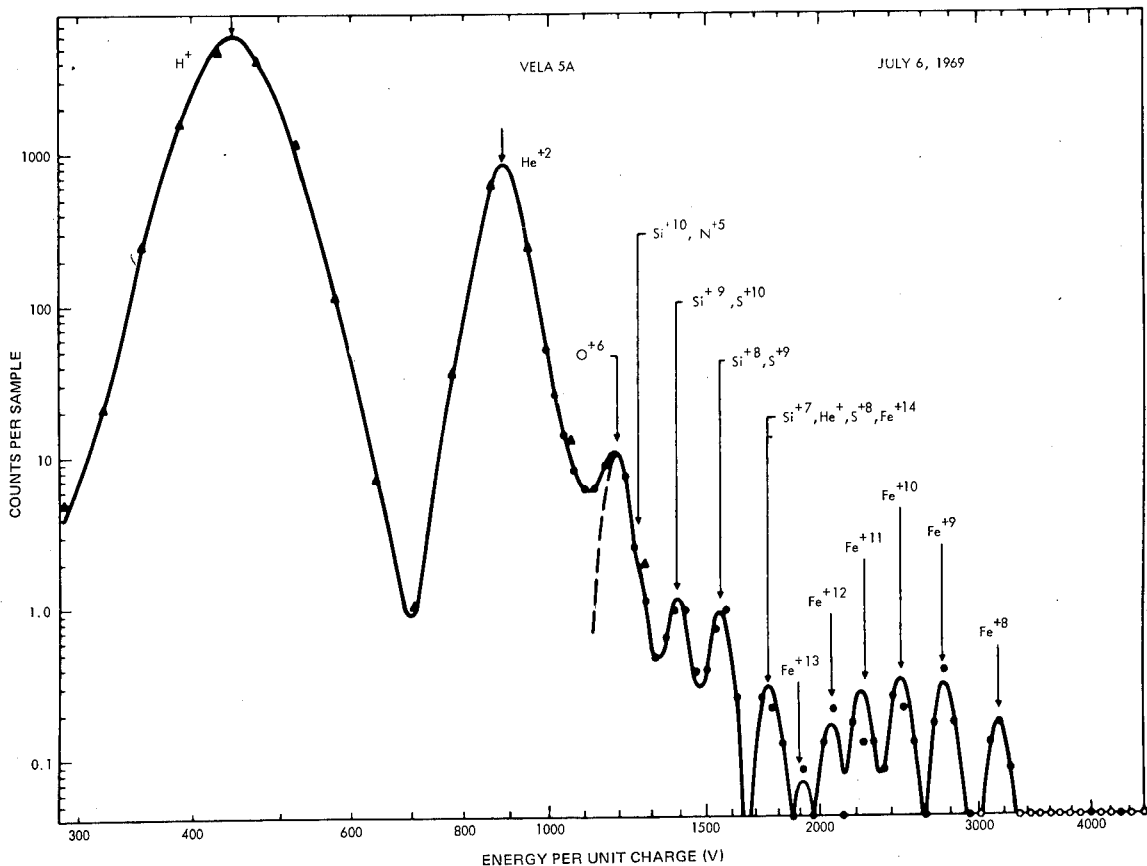


Figure 2.—Sample distribution of ion species in the solar wind near 1 AU. Data measured 6 July 1969 by the solar wind (triangles) and heavy ion (dots) analyzers on Vela 5A (refs. 11 and 12).

*Highest values ever reported for wind speed (1000 km/s), proton concentration (200 cm^{-3}), and magnetic field (30 nT), Neugebauer (1973, private communication). The extreme values observed in August 1972 are well-documented by Scarf, F. L. and Wolfe, J. H. in *J. Geophys. Res.*, vol. 79, no. 28, 1974, pp. 4179-4185 and by Mihalov, J. D. et al. in *Proceedings of the 7th ESLAB Symposium*, ed., D. E. Page, D. Reidel Co. (Dordrecht, Netherlands) 1974.

are negligible in comparison to protons in concentration and in mass and energy flux, they are not considered here. Histograms for the concentration, flow speed, direction, and temperature of the He^{++} ions strongly resemble those for the protons if the proton concentrations are multiplied by about 0.05 (this an extremely variable ratio). The temperature of the He^{++} ions is four times that of the protons. Thus, both flow and thermal velocities are approximately independent of ionic specie in the solar wind.

2.1.3.3 Electrons

Montgomery (ref. 13) reviews the available electron data. These data imply that the electrons participate in the bulk flow with velocity identical to that of local ions and with the concentration required for charge neutrality. The corresponding electron concentration and flow histograms are thus comparable to those shown in figure 1 for the protons and vary in phase with the protons. The electron temperature, however, is less variable than the proton temperature. Because electron temperature is almost always between 10^5 and 2×10^5 K with negligible anisotropy, the electron kinetic energy distribution, which peaks near 20 eV (for higher energies, see sec. 2.3.6), is primarily thermal rather than associated with the plasma flow. Average values and typical ranges from the literature are adopted for this monograph (table 2, sec. 3.1).

2.1.3.4 Magnetic Fields

Figure 3 includes histograms of magnetic field strength and orientation from discussion in reference 14. Common magnitudes for this highly variable field are about 5 ± 3 nT (5 gamma, or 5×10^{-5} Gauss) and may have any direction. On the average, directions inward or outward along a line about 45° west of the Sun, are more common. The field reverses average direction rather abruptly at irregular intervals (typically one week) and is consistent with the spiral and sector structure expected theoretically (sec. 2.1.1).

2.1.4 Dynamics

Significant correlations among proton concentration, flow speed, and temperature are shown in figure 4 (adapted from data reported in ref. 9). Similar correlations are discernible in measurements on almost any time scale from seconds to days. They are commonly discussed in terms of plasma streams that originate near the Sun, are related to solar activity, and move radially away. Among such plasma streams, high concentrations generally accompany low flow speeds and proton temperatures so that mass and energy fluxes in the solar wind are more nearly uniform than either the concentration or flow speed. The concepts of such streams and interactions among them (particularly when a fast stream overtakes a slow one) modify the simple theoretical picture (sec. 2.1.1) of the solar wind and magnetic field and lead to some understanding of the large variations seen in the plasma and field configuration data (ref. 15 and other sources).

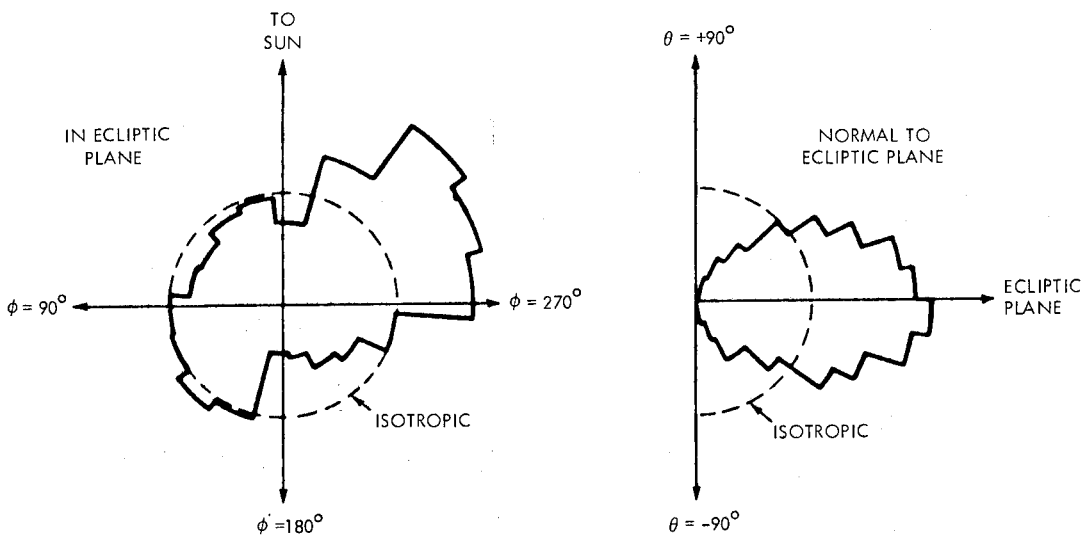
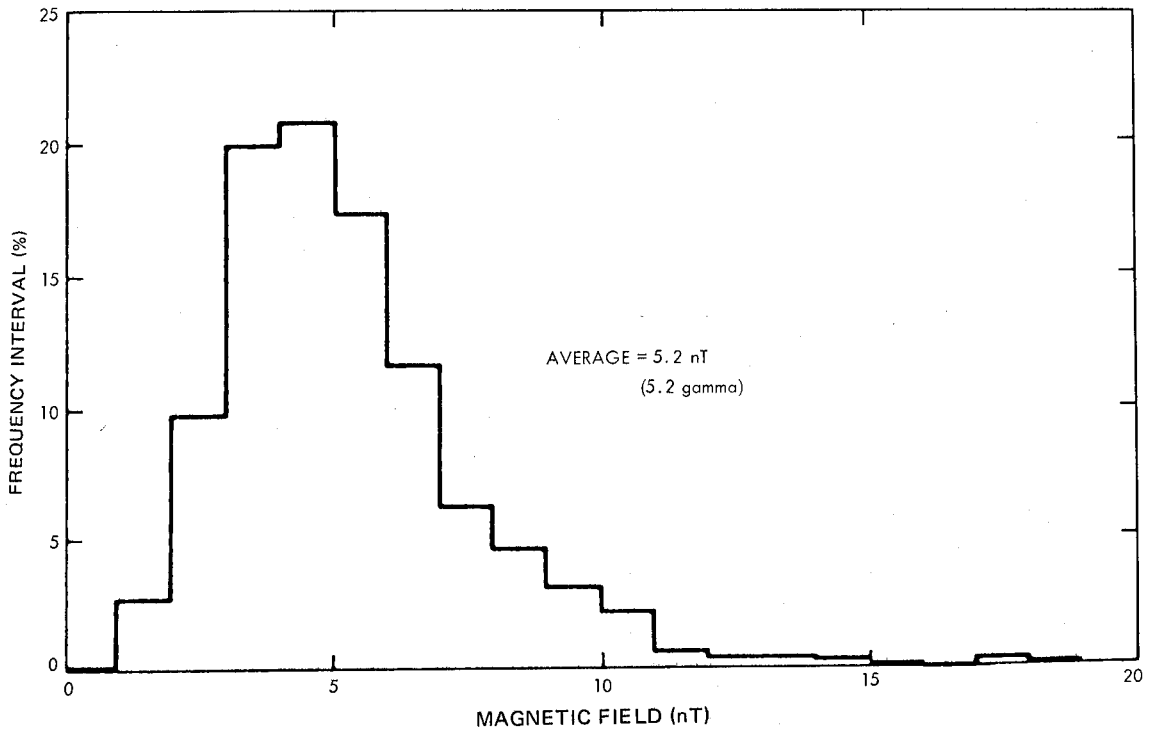


Figure 3.—Sample distribution of magnetic field strength and direction in the solar wind near 1 AU. Data measured in 1965-1967 by the magnetometer on IMP 3 (ref. 14).

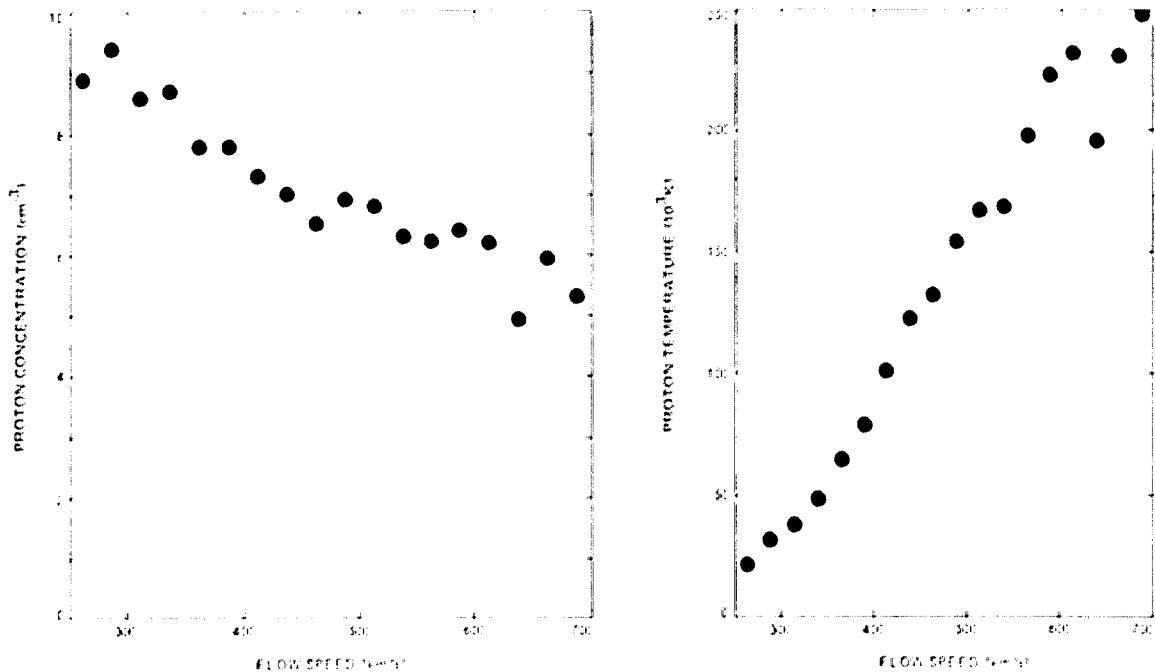


Figure 4.—Sample correlations among proton characteristics in the solar wind near 1 AU. Data sources identical to those for figure 1 (ref. 9).

A complementary view of the dynamics of the solar wind is provided by a look at the various time scales for variations in solar wind properties. Variations that occur on time scales less than or of the order of an hour (the microstructure) serve as data bases for the understanding of detailed interactions (including waves) in the solar wind and represent convection past the observer of volumes with different plasma properties (ref. 16). Variations on time scales of the order of a week (large scale and sector structure, sec. 2.1.1) represent the rotation past the observer of stream source regions on the solar surface with a period of about 27 days (ref. 10). Variations on time scales of a few years could be associated with the 11-year cycle of solar activity although predictions of specific variations in solar wind properties are not practicable on a long-term basis. However, available data indicate that the variations within a few days cover the full range of plasma properties that are seen associated with longer cycles.

2.1.5 Position Dependences

Spacecraft observations carried out between the orbits of Venus and Mars display no significant variation of the plasma velocity and temperature distributions with heliocentric distance S , but the concentration distributions are consistent with an S^{-2} dependence (ref. 17). These results are limited by the large variability in solar wind properties at one value of S (namely the Earth's orbit) and by the relatively small range of S values available to the experiments. They are generally consistent with a variety of theoretical analyses among which reference 18 is helpful because of its emphasis on variations with distance S and its

citation of most other prominent analyses. In interplanetary space, i.e., more than several radii from the Sun, simple power law dependence on distance is adequate for present purposes so we adopt proportionalities of S^{-1} for the magnetic field strength (appropriate for the two non-radial components), $S^{-1 \pm 0.5}$ for temperatures, and S^{-2} for concentrations. Plasma velocity is taken as invariant with distance S .

Likely dependences on solar latitude are ignored because they are unknown and probably smaller than the range exhibited by the variability with time.

The following information and considerations are of further interest to spacecraft design. Derived parameters of energy, flux, and pressure for the components of the solar wind are evaluated in table 2, section 3.1. For spacecraft surfaces not directly exposed to the solar wind flow, i.e., in a partially shielded location or on the lee side of the spacecraft (in the wake), the electron flux is not affected because electron thermal speeds exceed the relative velocity whereas protons are absent because their thermal speeds are much less than the relative velocity. This theoretical expectation applies unless spacecraft potentials exceed about 1 keV; then, detailed considerations of spacecraft configuration and space charge are required. Spacecraft potentials that may develop in space are discussed in NASA SP-8111 (Assessment and Control of Electrostatic Charges).

2.2 Galactic Cosmic Rays

Galactic cosmic rays are relativistic charged particles (electrons and atomic nuclei) that continuously penetrate the solar system from external sources in contrast to those that originate in the solar system. Individual particle energies range upward from about 1 to 10^{14} MeV, and typical energy densities for the entire population are in the range of 10^{-13} J/m³ which is comparable to the energy density of electromagnetic radiation from non-solar sources. In the literature cosmic rays are commonly described in rigidity rather than in energy terms (apps. A and B).

2.2.1 Observations

At the highest energies observed ($\gtrsim 10^{10}$ MeV), the intensity of cosmic rays is so small ($\lesssim 10^{-8}$ m⁻² s⁻¹ sr⁻¹) that it is impossible to record enough primaries for statistical significance with direct detectors of reasonable exposure. However, such particles do reach the Earth's atmosphere with negligible interplanetary or terrestrial magnetic field deflection and react with nuclei of air molecules to produce numerous secondaries in the form of extensive air showers (EAS) that can be analyzed with an array of ground-based scintillation detectors. This technique, reviewed in reference 19, effectively employs a large area of the atmosphere to provide sufficient exposure but does not permit the unambiguous identification of the primary cosmic ray particles.

At intermediate energies (10^4 to 10^9 MeV), data from ground-based instruments is supplemented by balloon-borne and to some extent by spacecraft experiments. Although any material may be examined for the effects of cosmic ray impact (ionization or nuclear

reactions), calibrated detectors (emulsion stacks, spectrometers, calorimeters, Cerenkov counters, and scintillators) provide the most detailed data. The ratios of protons and helium nuclei are very similar to those at lower energies, and the proportions of heavier nuclei, although possibly enhanced at higher energy levels, are still very small. The integral intensity determined from data at intermediate and high energies is reproduced in figure 5 (ref. 19).

At low energies ($\leq 10^4$ MeV), the particle intensities are affected by interplanetary and terrestrial magnetic fields and so depend on time and location of measurement. Consequently, detectors near the Earth's surface, particularly neutron monitors, measure fluxes of secondary particles produced in the atmosphere that depend strongly on latitude and less strongly on time of day. These monitors can also show counting rate enhancements during solar particle events, Forbush decreases (when solar wind streams near the Earth deflect low-energy particles), and variation with phase of the solar cycle. Numerous other detection systems for the low-energy particles and their secondaries have been deployed near the ground and within Earth's atmosphere and magnetosphere.

More reliable data on interplanetary intensities of low energy galactic cosmic rays have been derived from experiments on spacecraft beyond the influence of the Earth's atmosphere and magnetic field. These data come from cosmic ray telescopes on IMP, OGO, Mariner, Pioneer, and Soviet spacecraft. This instrument consists of an array of shielded Geiger-Müller counters, ionization chambers, solid state detectors, scintillators, and Cerenkov detectors with appropriate pulse height coincidence, anti-coincidence, and geometric analysis. After corrections for background noise and solar particles, the intensities are isotropic and in broad agreement among the numerous experiments; appropriate sample values for three different years are shown in figure 6 (ref. 20); the maximum integral proton flux corresponding to these data is about $3 \times 10^3 \text{ m}^{-2} \text{ s}^{-1}$.

These experiments are sometimes configured in ways that permit discrimination among electrons, positrons, protons, and several heavier nuclei. Among primary cosmic ray particles, protons predominate whether comparisons are made on the basis of rigidity, kinetic energy per incident particle, or kinetic energy per nucleon. Quantitative comparisons are commonly made on this last basis; an example is a useful, brief review in reference 21 from which figure 7 is taken for helium and other nuclei. Figure 8 from reference 23, provides comparative differential intensity spectra for electrons, positrons, protons, and helium nuclei.

2.2.2 Theory

Theoretical discussions of galactic cosmic rays commonly treat their composition, energy spectrum, and modulation which are among the characteristics that can be observed. These analyses treat particle origin and acceleration, e.g., Simpson (ref. 21); transport and containment in the galaxy and interaction with interstellar matter, e.g., Fichtel and Reames (ref. 24); and convection, diffusion, and other propagation effects in interplanetary space, e.g., Jokipii (ref. 25). For all these topics, however, there are major unresolved problems, and the theories do not greatly assist in the development of an engineering-oriented

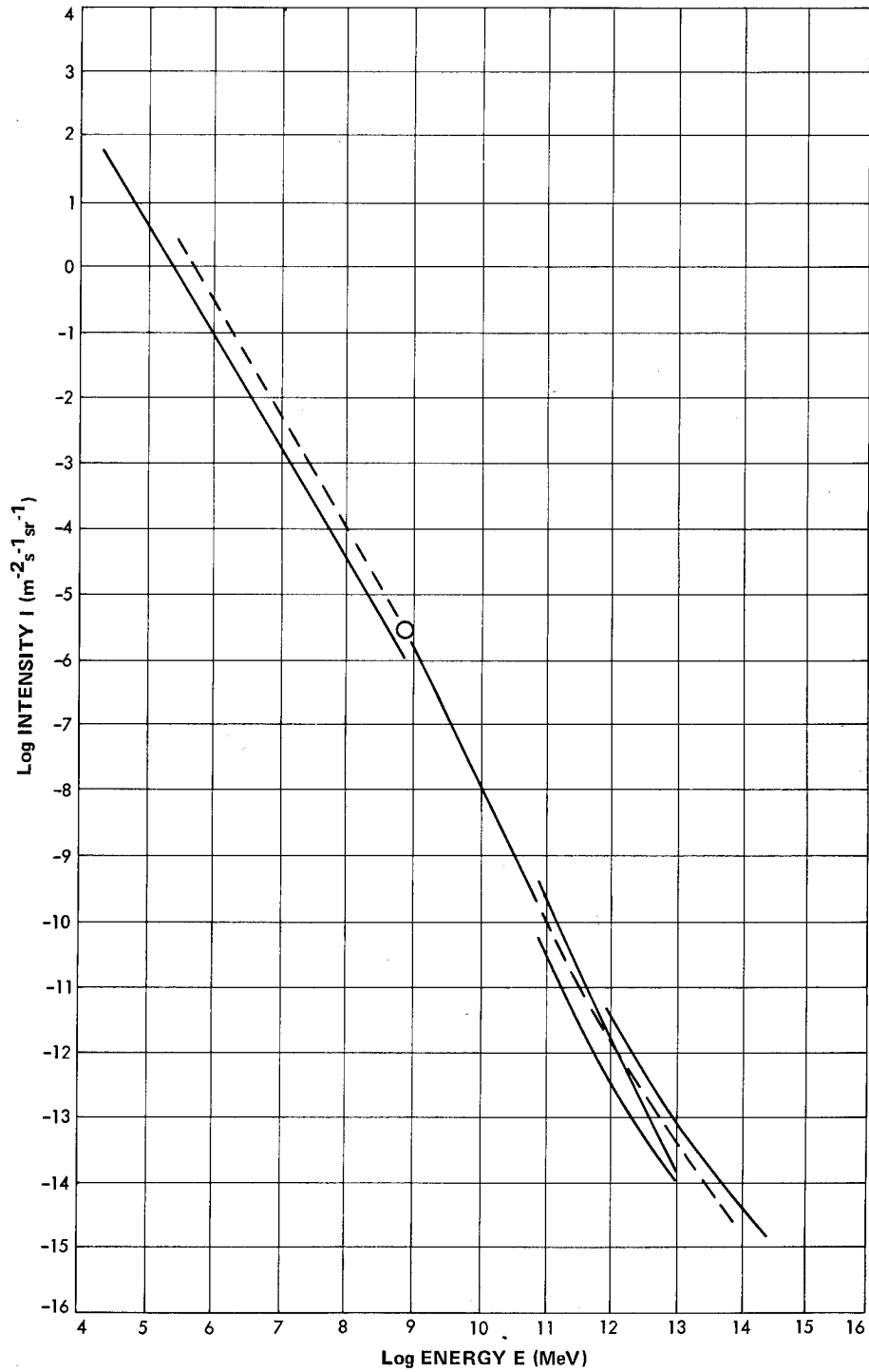


Figure 5.—Composite integral intensity spectra of primary galactic cosmic rays. The entries and their sources are reviewed by Sreenkantan (ref. 19).

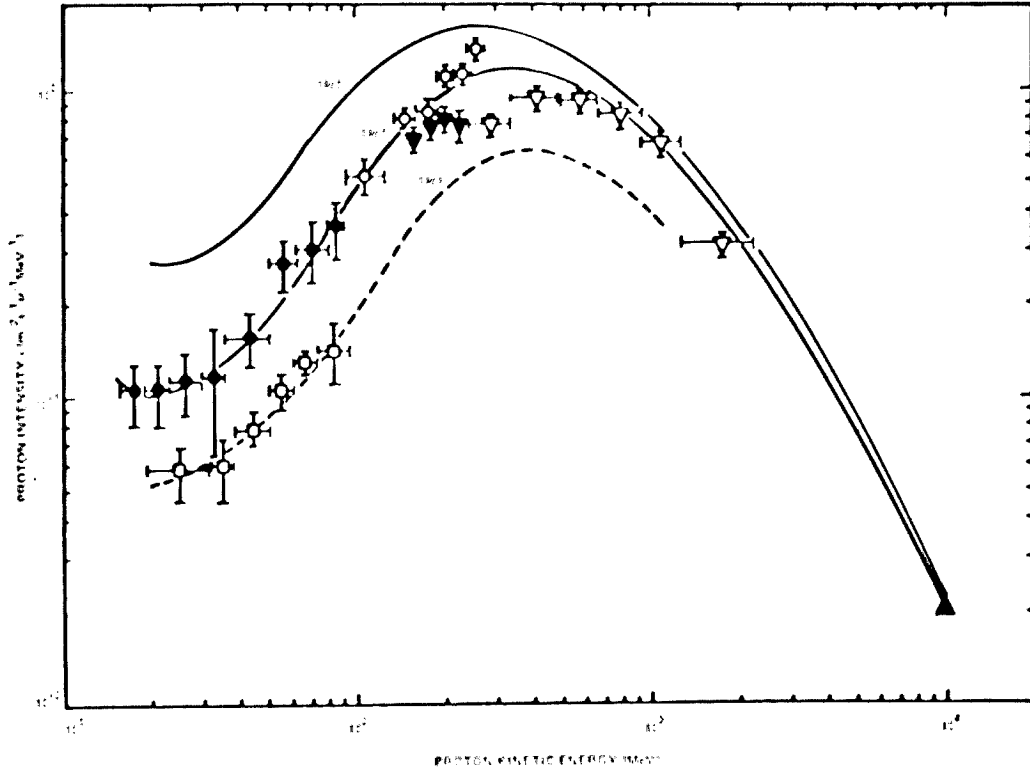


Figure 6.—Composite differential intensity spectra of galactic cosmic ray protons. The entries and their sources are reviewed in reference 20.

environmental description that is based simply on observations. In particular, heliocentric distance variations that might support the interplanetary transport models have not been confirmed by current data. (sec. 2.2.4).

2.2.3 Numerical Representations

For present purposes, instead of theoretical spectra for the components of galactic cosmic rays, we describe the intensities with ad hoc numerical expressions which approximate the data displayed in figures 5, 6, and 8. Such an expression for the integral electron intensity I_e is

$$I_e = \frac{2000}{(aE^6 + \beta E^3 + E^2 + \gamma)^{1/4}} + \frac{400}{E^{3/2}} \quad (1)$$

and its derivative that specifies the differential electron intensity i_e is

$$i_e = \frac{500(6aE^5 + 3\beta E^2 + 2E)}{(aE^6 + \beta E^3 + E^2 + \gamma)^{5/4}} + \frac{600}{E^{5/2}} \quad (2)$$

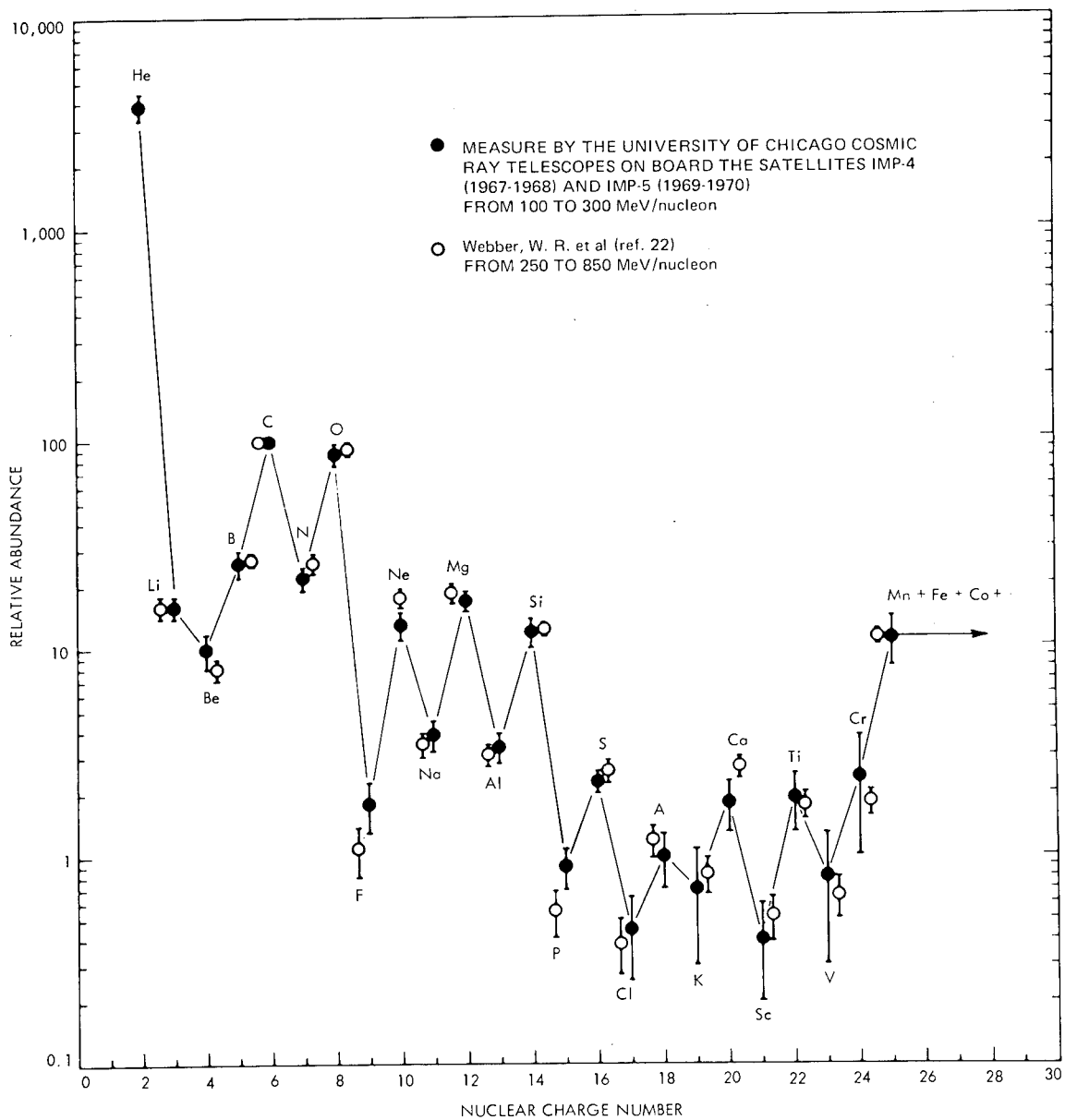


Figure 7.—Relative abundances (Carbon = 100) of cosmic ray nuclei at energies below 1000 MeV/nucleon as measured by IMP 4 and 5 (ref. 21).

Here the required units are E in MeV, I_e in $m^{-2}s^{-1}sr^{-1}$, and i_e in $m^{-2}s^{-1}sr^{-1}MeV^{-1}$; values of $\alpha = 10^{-12}$, $\beta = 10^{-3}$, and $\gamma = 6 \times 10^4$ yield intensities that match the mean of the observed data (fig. 8) to 25% or better at every electron energy in the range $1 < E < 3 \times 10^5$ MeV. Within a factor of 2, the positron intensities are 0.1 times the electron intensities (eqs. 1 and 2) at the same energy.

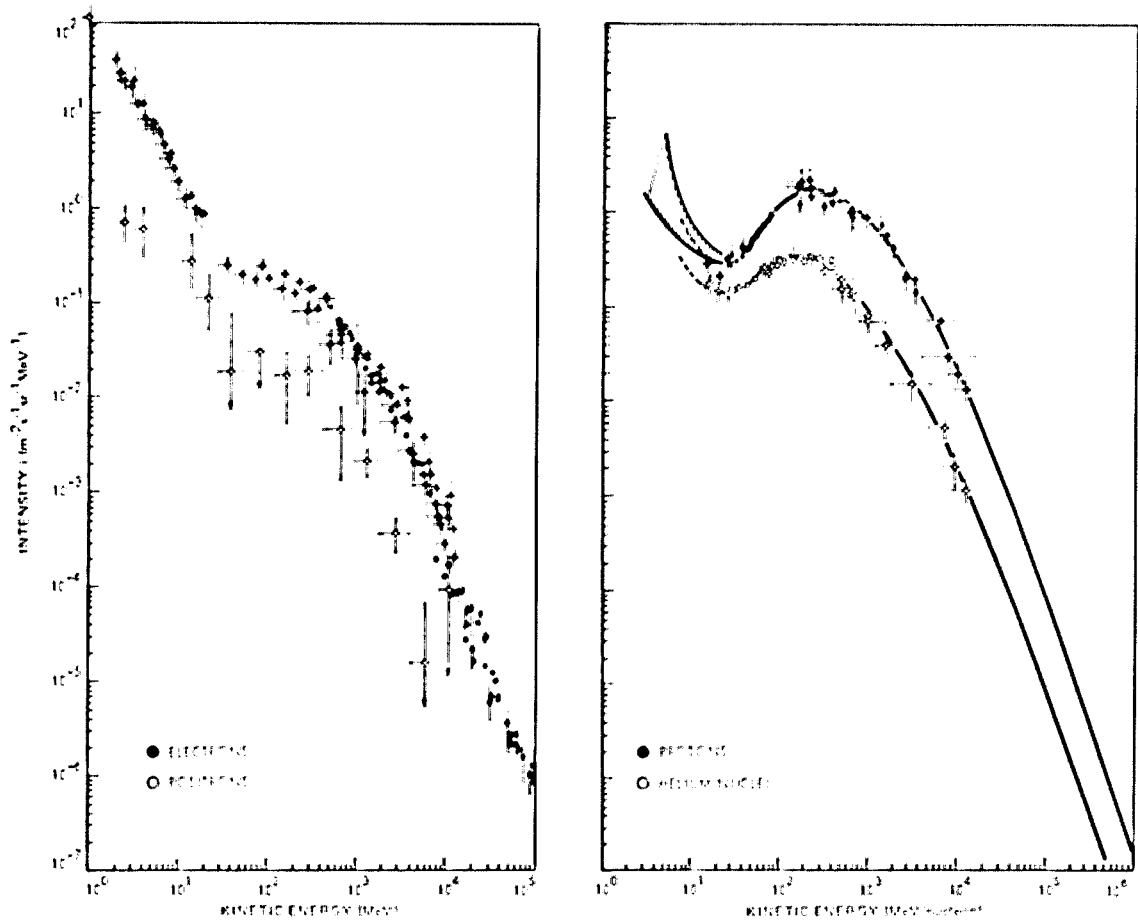


Figure 8.—Composite differential intensity spectra of galactic cosmic ray electrons, positrons, protons, and helium nuclei. The entries and their sources are reviewed in reference 23.

For the protons, comparable expressions are

$$I_p = \frac{3 \times 10^5}{[aE^6 + \beta E^4 + E^2 + (1.8)E_2^2]^{2/5}} + \frac{10^7}{E^{3.5}(E + \gamma E_2^2)} \quad (3)$$

and

$$i_p = \frac{1.2 \times 10^5 (6aE^5 + 4\beta E^3 + 2E)}{[aE^6 + \beta E^4 + E^2 + (1.8)E_2^2]^{7/5}} + \frac{10^7 [(1.6)E + (0.6)\gamma E_2^2]}{E^{8.5}(E + \gamma E_2^2)^2} \quad (4)$$

Here the required units are the same as for electrons; and values of $\alpha = 9 \times 10^{-29}$, $\beta = 5 \times 10^{-9}$, and $\gamma = 8$ yield intensities that match the mean of the observed data (figs. 5 and 6) to 50% or better at every proton energy $E > 20$ MeV. Here also E_2 is the energy at which i_p is maximum; and for the best fit to figure 6, the values 300, 400, and 550 MeV should be assigned to E_2 in 1965, 1967, and 1969, respectively. The intensities of other nuclear

species may be approximated for the same values of energy E in MeV/nucleon, by multiplying the proton expressions by the values listed in table 3 (sec. 3.2) and contained in figures 7 and 8.

2.2.4 Time and Position Dependences

The modulation of the intensities of galactic cosmic rays imposes variations up to an order of magnitude on the low energy ($\lesssim 100$ MeV) particles on a time scale of a few years (fig. 6). Even though the most plausible explanation involves the interaction of the galactic cosmic rays with interplanetary magnetic fields controlled by the solar wind, quantitative correlations with solar activity indicators are not reliable even over the short time span from 1965 (near solar minimum) to the present (well beyond solar maximum). Thus, as an ad hoc technique for representation of past data and predictions for spacecraft design, values for E_2 (energy parameter in the proton fit, sec. 2.2.3) are suggested as follows:

$$E_2 = \begin{cases} 576 - |64(t - 1970)| & \text{for } 1964.75 \leq t \leq 1975.25 \\ 576 - |64(t - 1980.5)| & \text{for } 1975.25 \leq t \leq 1985.75. \end{cases} \quad (5)$$

Here E_2 is in MeV, t is the date in years, and a solar cycle of 21 years (half-cycle 10.5 years) has been assumed. This representation for E_2 is shown in figure 13 (sec. 3) and approximately reproduces the E_2 values cited in section 2.2.3.

Spacecraft data for deriving the variation of galactic cosmic ray intensities with heliocentric distance near Earth give very diverse and possibly energy-sensitive results. (References 26 and 27 suggest that data associated with a baseline of a few tenths of an astronomical unit are not appropriate for establishing a reliable relationship between galactic cosmic ray intensities and heliocentric distances.) The Pioneer 10 observations with a baseline that extends to 4 AU from the Sun have given a null result for variation of the intensity of protons above 80 MeV with heliocentric distance (ref. 28). It has further been demonstrated that, at low energies, theory permits several very different interstellar cosmic ray spectra (ref. 29) to match observed ones near the Earth after modulation by convection, diffusion, and other mechanisms. Thus, it is difficult to rationally select an interstellar spectrum and a corresponding description for the transition from 1 AU to interstellar space. We adopt here the simplest description consistent with the observations, i.e., in all interplanetary space, cosmic ray intensities and their energy spectra are identical to those observed just beyond the Earth's magnetosphere. This is equivalent to assuming a modulation region that is large compared to the Earth's orbit within which cosmic ray intensities are uniform in space but variable with time. In this modulation region, the intensities would be rather different at low energies than the presumably time-independent intensities in interstellar space.

Data on the time and position dependences of the electron component of cosmic rays, e.g., Earl (ref. 30) and Schmidt (ref. 31), are less thoroughly developed than for the protons so we adopt the spectra specified by equations 1 and 2 for all interplanetary times and positions.

2.3 Solar Particle Events

Occasionally protons with energies of the order of 10 to 100 MeV propagate in interplanetary space after acceleration near the Sun. This phenomenon is called a solar particle event and generally occurs subsequent to flares on the Sun's surface. The flare eruption and proton acceleration and release probably share an origin in local instabilities of the plasma and magnetic field configurations within active regions on the Sun that are usually associated with sunspots. Such protons are referred to as solar flare protons or solar cosmic rays. Associated electrons are discussed in section 2.3.6.

2.3.1 Observations

The presence of energetic solar particles near the Earth has been inferred from various ground-based instruments, notably neutron monitors, ionization chambers, riometers, and from charged particle detectors carried in balloons, aircraft, and satellites. The data so acquired, however, include modifications that result from particle interactions with the Earth's magnetosphere and atmosphere. More direct data are fortunately available from charged particle detectors on IMP spacecraft (Earth-orbiting satellites with apogees outside the magnetosphere) and on Pioneer spacecraft (that operate in interplanetary space). Some protons in the energy range of interest are commonly present. However, flux enhancements from solar protons of several orders of magnitude occur in relatively distinct events at very irregular intervals. In many months no events are detected, but in others one to six occur so an average rate is of the order of one event per month.

During an event, particle intensities peak at some particular energy after a rapid rise, commonly of a few hours, and decrease more slowly until disappearance, commonly after several days. The time profiles and the development of the spectra are of great variety and are affected by the individual event and the detector trajectory (ref. 32). The integration of the intensity from all directions and over the duration of the event leads to values for the fluence at various proton energies. Recurrences of proton detection after about 27 days (one solar rotation) have also been observed, but the recurrent intensities are orders of magnitude smaller than the original ones.

The angular distribution derived from charged particle telescope data are strongly variable as well, according to summaries, e.g., reference 33. The anisotropy commonly ranges between 0.2 and 0.5 early in an event with the variable direction of maximum intensity often parallel to the interplanetary magnetic field. Later in the event after the peak intensity, the anisotropy is commonly smaller, e.g., 0.1, so a more nearly isotropic intensity is indicated. Because the dependence of the intensity on direction is so variable and because the intensities are so variable in time and the events are so sporadic, it is not worthwhile to include directional effects in an engineering model as their variations are masked by other uncertainties.

2.3.2 Theory

Several authors have discussed mechanisms for processes near the Sun that result in particle acceleration, storage, injection, and leakage. However, it is difficult to judge the validity of

these mechanisms on the basis of observed particle populations. This is because the population of the particles undergoes major modifications through various phenomena of particle transport in space. These phenomena include convection, adiabatic deceleration, anisotropic diffusion, interaction with a diffusion region external boundary, and possibly others. Their theoretical treatment is commonly handled with a Fokker-Planck equation; the complexity of the relationships among position, time, energy, intensity, flux, and various input parameters, e.g., in the diffusion coefficients and boundary conditions, suggests that numerical solutions are appropriate. Aspects of such theories, their development in the literature, their numerical solutions, and comparisons with the observations are given in references 34, 35, and elsewhere.

Both the complexity of the theory and the individuality of particular events suggest that the above successful theoretical and numerical treatments are not suitable for the overall engineering descriptions needed here. Therefore, we view the peak intensity and fluence for an event as functions of energy and heliocentric distance, irrespective of the time profile or the angular and heliocentric longitude dependences. Near the Earth's orbit, average energy spectra for numerous solar particle events can be obtained from spacecraft observations. However, only a few events have been observed at widely-separated positions so that inferences about position dependences are confused by the individuality of the events observed. Furthermore, the position dependences may differ at different energies because the relevant transport mechanisms assume different relative importances.

To provide a suitably simple model, three ad hoc assumptions, only loosely tied to the results of the theoretical treatments, are adopted here. First, particle acceleration and loss in interplanetary space are ignored so that energy spectra are independent of position. Second, any angular spreading of the particles (as they move a distance S from the Sun) is ignored so that, to avoid long-term changes in the particle content of interplanetary space, a fluence proportional to S^{-2} applies to events on the average. Third, to account for more rapid diffusion in the general direction of the particle trajectory than perpendicular diffusion, the radial extent of a group of particles is taken as proportional to S so that the peak intensity is proportional to S^{-3} (inversely proportional to the volume occupied by the particles) for events on the average. Some alternate, energy-dependent relations, and further references are discussed by Thomas (ref. 36) and Haffner (ref. 37); for $S > 1\text{AU}$, the dependences used in this monograph predict equal or higher intensities than references 36 and 37.

2.3.3 Data Availability

Tables that summarize data from many events on a common basis are needed to develop prediction schemes. Because there is strong correlation of these events with other various aspects of solar activity, the data are divided into solar cycles which are revealed by sunspot number maxima and minima with an approximate eleven-year periodicity. Prior to solar cycle 19, starting in 1954, insufficient data on solar protons are available for useful analysis. For cycle 19 (from 1954 to 1964) a data tabulation is provided by Weddell and Haffner (ref. 38) that extends the ground-based, balloon, and satellite data compiled by Webber (ref. 39) through 1963. For cycle 20 (from 1964 to the present) data tabulations are provided by Atwell (ref. 40), Yucker (ref. 41), and King (ref. 42), mainly on the basis of IMP and Explorer spacecraft observations. Because cycle 19 was exceptionally active (unlike

expectations for the following several cycles, notably 20 and 21) and because available data exhibit poorer internal consistency than for cycle 20, King (ref. 42) argues convincingly that cycle 20 data alone form an appropriate basis for predictions.

Some of the foregoing data compilations and others include various other facets of solar activity, e.g., observed details of associated sunspots, flares, plages, and radio frequency bursts. Correlations of such data with solar particle event observations permit short-term predictions of solar particles on time scales from weeks to hours in advance with modest accuracy. Such predictions are useful in spacecraft operations (ref. 43). For spacecraft and mission design purposes, however, long-term predictions are needed. Available techniques quantify the correlations of event probability of occurrence and severity with solar activity and use the results for prediction purposes; leading examples are references 36, 41, 44, 45, 46, and 47. Certain features from these articles have been included in the recent development of a complete probabilistic description by King (ref. 42).

In sections 2.3.4 and 2.3.5 a modification of King's technique is adopted which includes the following features: solar particle event data from cycle 20 alone; continuous (rather than discrete) values for energy, intensity, fluence, and probability; and applicability to interplanetary missions with arbitrary time profiles of heliocentric distance.

For rare solar events with substantial proton intensities at very high energies (near 1000 MeV) such as observed in cycles 18 and 19, section 2.3.6 provides a means for representation.

2.3.4 Application of Data to Mission Planning

King (ref. 42) has made a careful analysis of the cycle 20 events, with three major conclusions.

1. Most events (labeled OR, for ordinary) can be described by a log-normal distribution in event fluence. Although the parameters of such a distribution depend on the criteria used for selection of the data set, the chosen criteria do not greatly affect the mission fluence probabilities that are derived.
2. The events of August, 1972, which yielded most of the solar proton fluence observed in cycle 20, are representative of the most severe events in other solar cycles and belong to an event class distinct from the foregoing OR events. Such events King labels AI (anomalously large) and concludes that they must be treated separately from the OR events in any probabilistic description.
3. The separate contributions of AI and OR events to mission probabilities can be simplified to graphical and numerical techniques that permit facile computation of fluences for missions at 1 AU from the Sun during the seven most active years of cycle 21.

For the present purposes the foregoing conclusions have been adopted and extended in the following ways.

4. Points 1 through 3 above can be applied with minor modifications to the peak proton intensity during a mission.
5. The technique for both peak intensity and fluence can be modified to permit its use for missions that exceed the restrictions of point 3 above (i.e., extension to missions away from 1 AU and at any time in the solar cycle).

To implement these concepts, we first specify the log-normal distributions for the peak intensity and fluence of the cycle 20 events listed by King (ref. 42). Let x represent the common logarithm of the peak intensity I , and $p(x)dx$ represent the probability that I falls in the interval $(10^x, 10^{x+d_x})$, where

$$p(x) = \frac{1}{\sigma_I \sqrt{2\pi}} \exp [-(x - \langle \log I \rangle)^2 / 2\sigma_I^2]. \quad (6)$$

Similarly, where the symbol $\langle \rangle$ denotes average value, let y represent the common logarithm of the event fluence F , and $q(y)dy$ represent the probability that F falls in the interval $(10^y, 10^{y+d_y})$, where

$$q(y) = \frac{1}{\sigma_F \sqrt{2\pi}} \exp [-(y - \langle \log F \rangle)^2 / 2\sigma_F^2] \quad (7)$$

The parameters for these fits derived from the 12 largest among the appropriate OR event entries tabulated by King (ref. 42) are given in table 4 (sec. 3.3), where units $m^{-2}s^{-1}sr^{-1}$ and m^{-2} are associated with entries for I and F , respectively.

2.3.5 Long-Term Probabilities

Commonly for random, independent solar particle events, the Poisson distribution is used, e.g., Yucker (ref. 41). However, because the data base for cycle 20 events is so limited, the rate parameter basic to such a Poisson distribution cannot be precisely determined. Burrell (ref. 44) has shown that the appropriate distribution results from an extension of Poisson statistics to a small data set. The result, as presented by King (ref. 42), is

$$P(n, \tau; N, T) = \frac{(N+n)!}{N!n!} \frac{(\tau/T)^n}{[1 + (\tau/T)]^{N+n+1}} \quad (8)$$

where P is the probability that n events occur in a time interval τ on the basis that N events were observed in a comparable past time interval T .

To apply the foregoing distribution to the peak intensity observed for a mission of duration τ , consider the probability

$$P_1(I) = \int_{-\infty}^{\log I} p(x)dx \quad (9)$$

that if one event occurs its peak intensity is less than I . (We set aside energy dependence for simplicity.) The comparable probability $P_n(I)$ that if n events occur the peak intensity is less than I , is $P_n(I) = [P_1(I)]^n$. Thus the probability that the peak intensity for the mission exceeds I is simply

$$\sum_{n=1}^{\infty} P(n, \tau; N, T) \{1 - [P_1(I)]^n\}. \quad (10)$$

If we use the $N = 12$ events in $T = 7$ years which are described by equation 8, the probability specified in equation 10 is a function only of τ and I . It has been computed for several cases and is shown in figure 9 (sec. 3.3). Although the figure has been prepared for an energy threshold $E_p = 30$ MeV, reasonable results for other energy thresholds can be obtained by scaling with the $(\log I)$ values from table 4.

The analysis for the mission fluence is much more complex because every event contributes to the fluence. That analysis has been completed by King (ref. 42) who evaluates in figure 10 (sec. 3.3) the expression for fluence comparable to equation 10. However, in cycle 20 most of the fluence was contributed by the AI events in August, 1972, whereas the foregoing analyses consider only several OR events. Because of the difference between these two kinds of events, it is possible to distinguish two regimes, Regime 1 in which the OR events may be ignored and Regime 2 in which only the OR events contribute significantly. The separation between these regimes has been derived by King (ref. 42) as shown in figure 11, (sec. 3.3) where Regime 1 lies below and to the right of the curve labeled $N = 1$ and Regime 2 lies on the other side of this curve.

If the OR events are ignored, a very simple probability analysis results from equation 8 by consideration of AI events alone. On the basis that one event ($N = 1$) was observed in the time interval T (seven years) by considering the August 1972 data as one event, the probability that no events ($n = 0$) occur in a time interval τ is given through use of equation 8 as

$$P(0, \tau; 1, T) = [1 + (\tau/T)]^{-2}. \quad (11)$$

Thus, the probability that the peak intensity of the August 1972 events (table 4, sec. 3.3) be matched because one or more such events occur, is $[1 - P(0, \tau; 1, T)]$ as given by equation 11. This result is the basis of the $N = 1$ curve in figure 11 (sec. 3.3).

For Regime 1 where the major contribution is from AI events, the fluence associated with a particular probability level may be derived from one or more AI events. For this purpose, King (ref. 42) has derived figure 12, (sec. 3.3) from the appropriate combination of terms represented by equation 8, with $N = 1$ and $T = 7$ yr. To obtain a continuous representation of fluence as a function of probability one may interpolate in figure 12 (sec. 3.3) to find the number of AI events associated with a given probability and time interval and then multiply that number of events by the fluence entries in table 4 (sec. 3.3). This technique reproduces King's results for integer numbers of AI events.

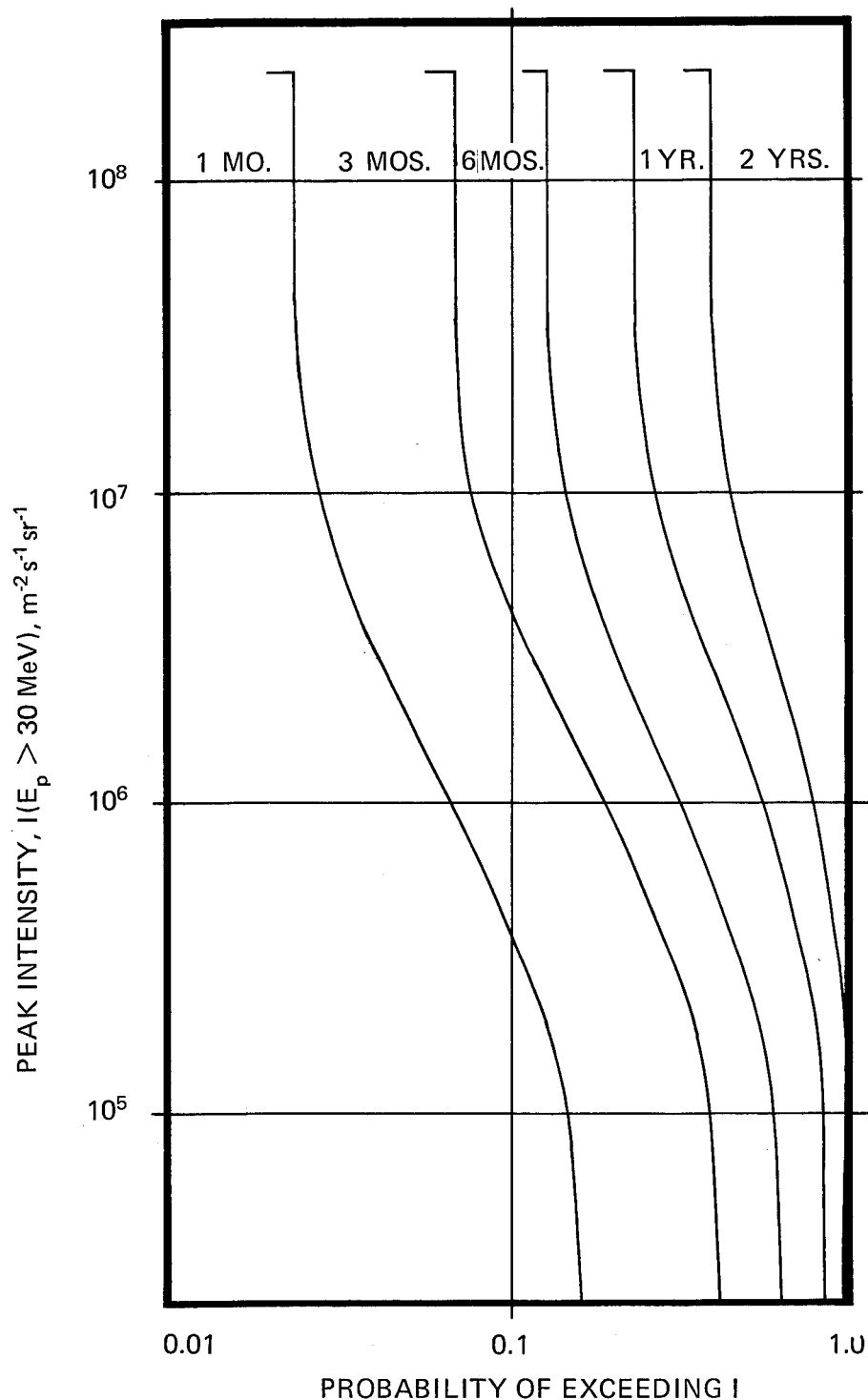


Figure 9.—Probability of exceeding peak intensity I of solar protons with energy $E_p > 30$ MeV, for missions of varying duration at $S = 1$ AU, and for intensities less than that associated with 1 AL event. (Intensity for 1 AL event is shown by horizontal bars.)

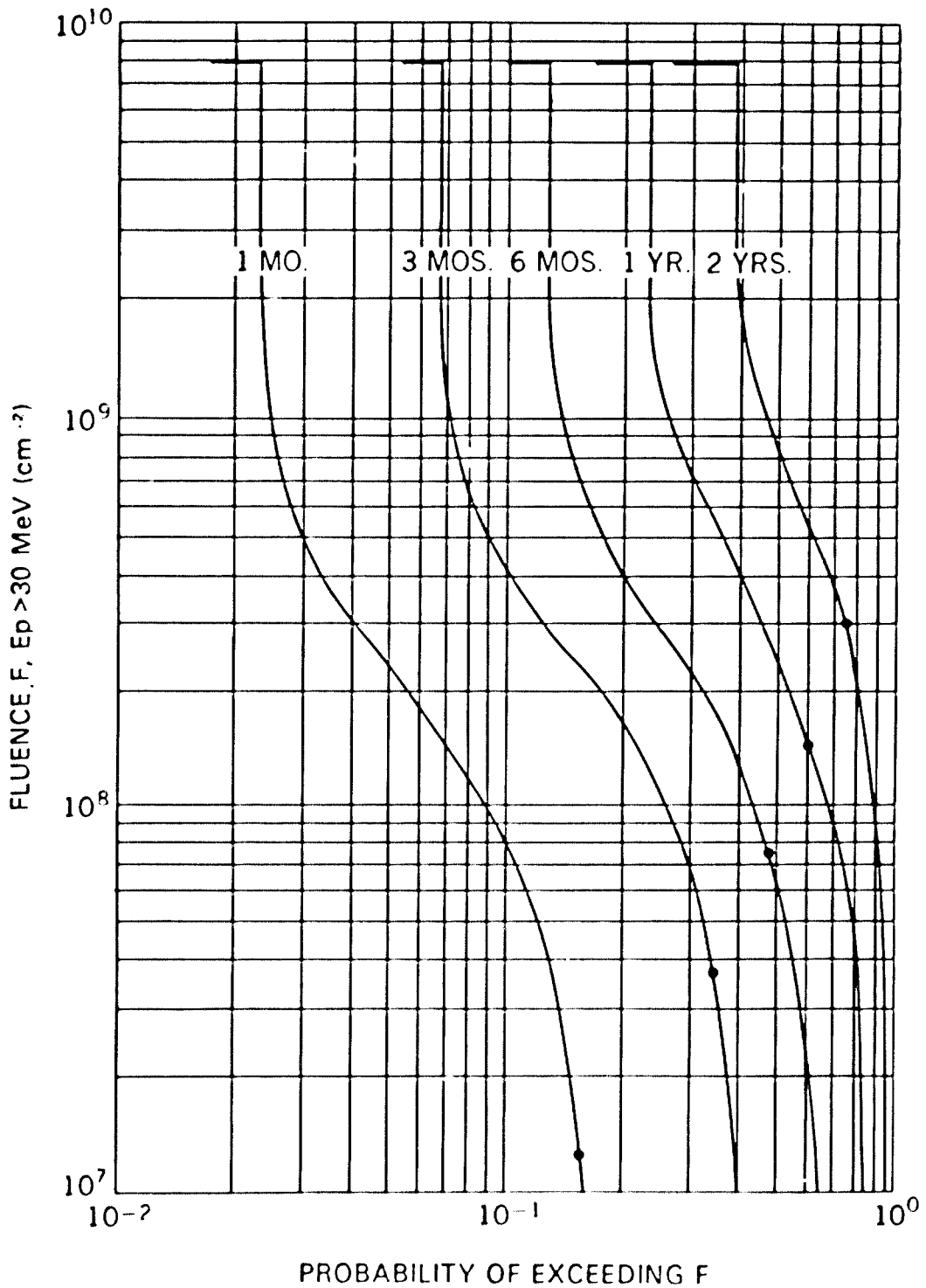


Figure 10.—Fluence of protons above 30 MeV that will be exceeded with probability, P, for missions of varying durations at S = 1 AU and for fluence levels less than that associated with one AL event. (Fluence for 1 AL event is shown by horizontal bars.) Heavy dots on each curve indicate galactic proton fluence to be encountered (from King, ref. 42).

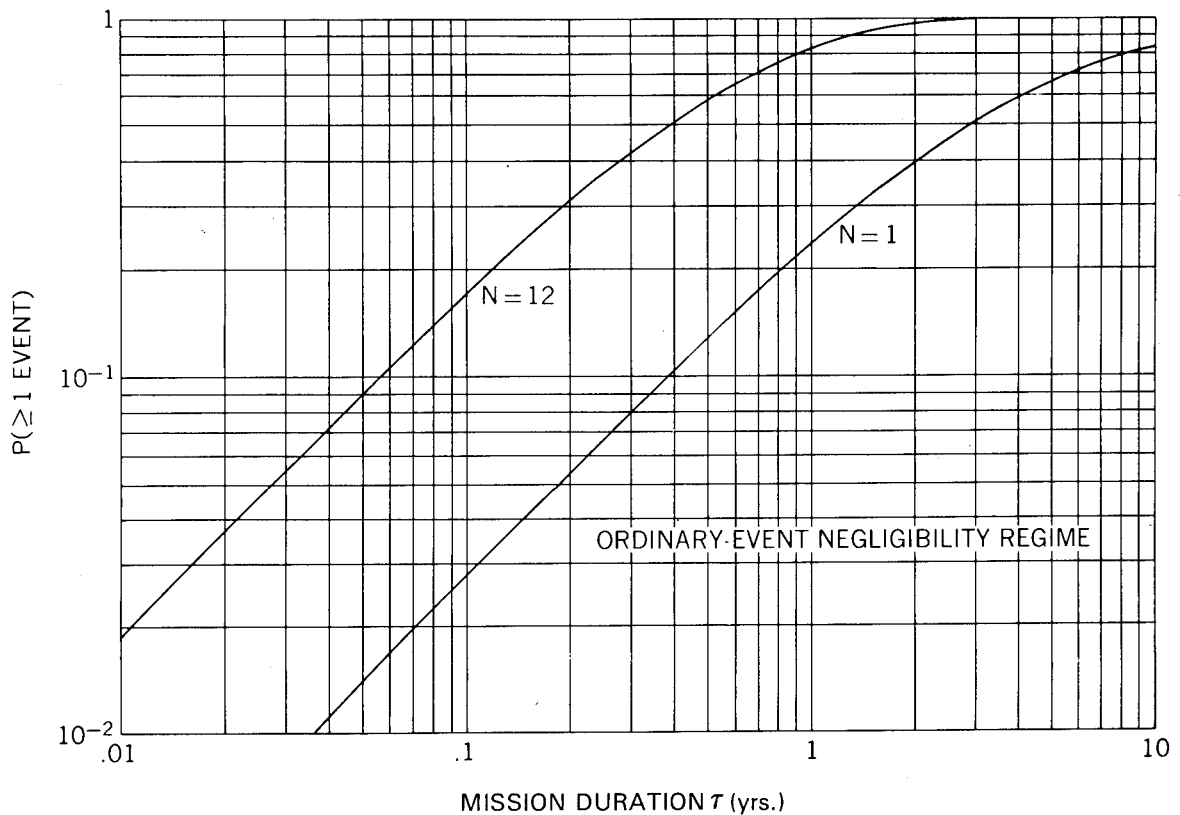


Figure 11.—Probability of observing at least one event for missions of duration τ given the past observation of one and twelve events in seven years (from King, ref. 42).

As a final modification of the foregoing analysis, we consider missions that encompass values of heliocentric distance $S \neq 1$ AU and time intervals ($t_1 < t < t_2$) that exceed the seven active years (1977-1983) anticipated for cycle 21. These two modifications can be effected by multiplying the results for intensity or fluence by

$$W_m = \frac{1}{(t_2 - t_1)} \int_{t_1}^{t_2} [S(t)]^{-m} f(t) dt. \quad (12)$$

The heliocentric distance variation comes from the considerations in section 2.3.2: the fluence at $S \neq 1$ AU is FS^{-2} so an integration as specified in equation 12 is appropriate when 2 is taken as the value of m . Similarly for the peak intensity, equation 12 should be applied for $m=3$. For the seven active years of the solar cycle, $f(t) = 1$ is consistent with the foregoing analysis. For the four years (1962-1965) of the solar minimum between cycles 19 and 20, both the frequency and severity of solar particle events are lower than for OR events between 1966 and 1972, and AL events are absent (refs. 41 and 42). An estimate of the frequency and severity ratios from the values derived by Yucker (ref. 41) and

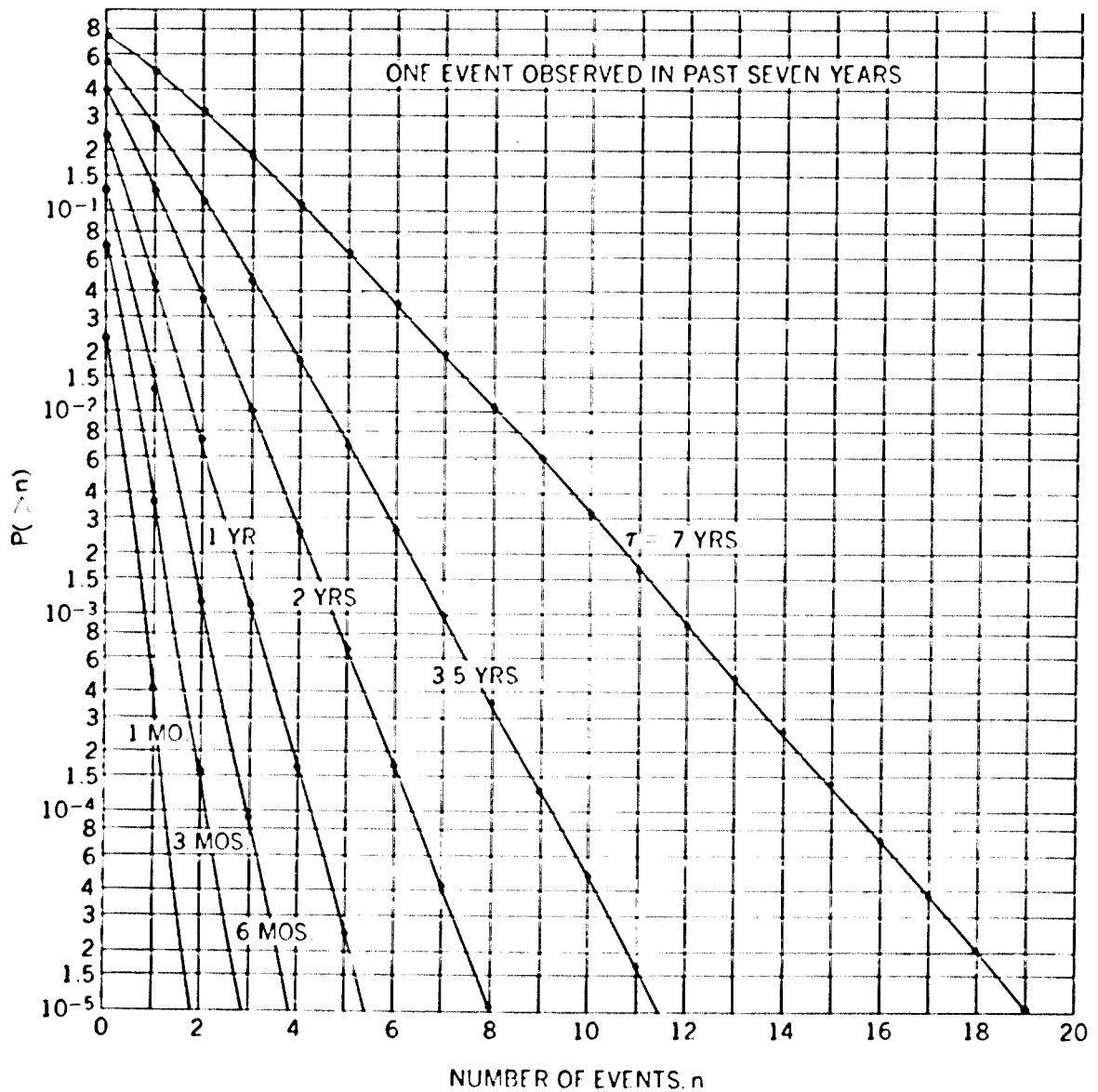


Figure 12.—Probability of observing more than n events in missions of varying durations given the past observation of one event in seven years (from King, ref. 42).

subsequent data suggest that $f(t) = 0.3$ is a reasonable upper limit for solar minimum: the reduced frequency can be simply included if we use

$$\tau = \int_{t_1}^{t_2} f(t) dt \quad (13)$$

for missions that occur partly or completely during solar minimum. The techniques of equations 12 and 13 permit extension of the analysis represented by equations 6 through 10 and figures 9 through 12 (sec. 3.3) to conditions away from $S = 1$ AU and solar maximum.

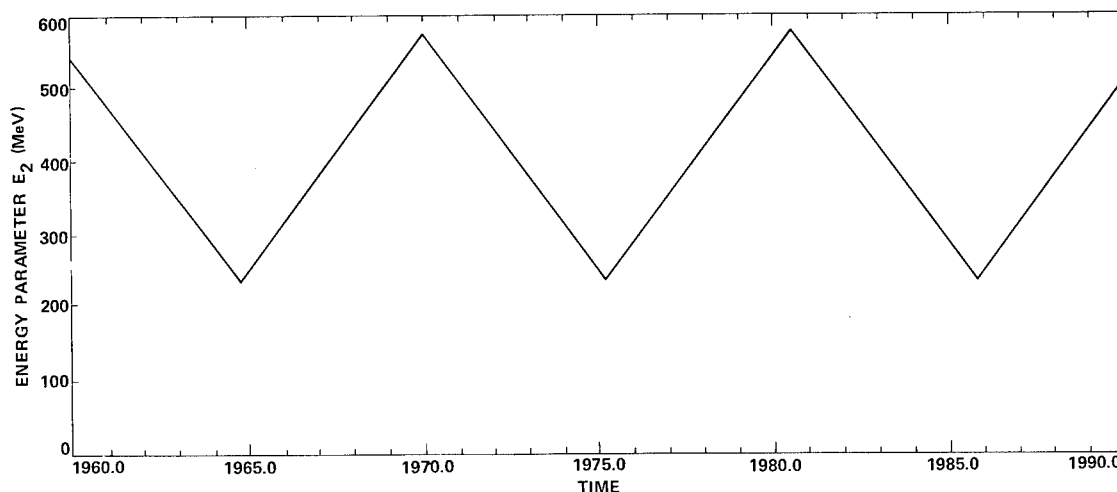


Figure 13.—Time-dependence of the energy parameter E_2 for the numerical representation of galactic cosmic ray proton intensities modulated by solar activity.

2.3.6 Other Particles and Energies

Components of solar particle radiation other than the solar wind and solar flare protons in the energy range of a few to a few hundred MeV are less fully treated in the research literature. Their development here is accordingly brief.

For energies from 100 MeV to about 1000 MeV, solar event data are rare, but an extrapolation of the description of sections 2.3.4 and 2.3.5 for solar protons is probably reasonable, particularly for OR events and for fluence estimates. At about 1000 MeV and above, primary galactic cosmic rays (sec. 2.2) dominate the environment except for rare, high-energy solar proton events. For the latter, near and above 1000 MeV, the largest intensities ever observed were included in the event of 23 February 1956 (cycle 19) for which a schematic spectrum is provided by Foelsche*; that spectrum can be represented (applying some of the considerations in the foregoing sections) as a peak intensity in the form

$$I = (4 \times 10^6 \text{ m}^{-2} \text{ s}^{-1} \text{ sr}^{-1})(E/1000 \text{ MeV})^{-\gamma} S^{-3}$$

where $\gamma = 0.7$ for $E < 1000$ MeV and $\gamma = 4$ for $E > 1000$ MeV. Occurrence of other high-energy events on 25 July 1946, 19 November 1949, 12 November 1960, and 30 March 1969 suggest that such events may be associated with rapidly increasing or decreasing solar activity rather than with the periods of peak activity in each cycle.

*Foelsche, T., "Radiation Measurements and Doses at SST Altitudes," NASA TMX-2440, 1972, pp. 894-901. Other compilations by Foelsche of high energy events are found in NASA SP-71, SP-169, and NASA TND-7715.

In the energy interval between the solar wind and solar proton events ($10^{-3} < E < 10$ MeV), a peak integral intensity of $I = (10^8 \text{ m}^{-2} \text{ s}^{-1} \text{ sr}^{-1})/S^3 E^{1.2}$ approximately matches both a high solar wind value and a typical solar proton event. In the same interval an average integral intensity of $I = (10^6 \text{ m}^{-2} \text{ s}^{-1} \text{ sr}^{-1})/S^2 E^{1.7}$ approximately matches both a typical solar wind value and average fluence accumulation rate from solar proton events. In these crude approximations the heliocentric distance S is in AU and the proton kinetic energy E is in MeV for the range $10^{-3} < E < 10$ MeV. The two proton enhancements reported for $5 \lesssim E \lesssim 20$ keV by Frank (ref. 48) had intensities intermediate between the average and peak values resulting from the foregoing two expressions.

Nuclei other than protons are present in solar particle events, but intensity ratios are less than or equal to that of helium for which an intensity 0.05 times that of the protons is reasonable for both the solar wind (sec. 2.1.3.2) and solar particle events (ref. 49); a range of 0.0 to 0.25 for this ratio includes most of the data.

Cline and McDonald (ref. 50) describe the 3 to 12 MeV electron component of several solar particle events that were observed by IMP 1 and 3. Typical peak intensities are $10^4 \text{ m}^{-2} \text{ s}^{-1} \text{ sr}^{-1}$ in this energy range for which McDonald *et al.* (ref. 23) feel a differential spectrum proportional to E^{-3} is appropriate. A peak integral intensity approximation, $I = (10^5 \text{ m}^{-2} \text{ s}^{-1} \text{ sr}^{-1})/S^3 E^2$, matches these properties and when extrapolated to lower energies is comparable to the largest observed intensity tabulated by Lin and Anderson (ref. 51) for electrons with energy $E > 40$ keV. If a duration of 10^4 seconds and a rate of the order of once per month are adopted for such a solar event electron intensity, an average integral intensity approximation, $I = (400 \text{ m}^{-2} \text{ s}^{-1} \text{ sr}^{-1})/S^2 E^2$, is comparable both to the galactic cosmic ray electron intensity above 1 MeV (some of these may be solar as discussed in ref. 23) and to the intensity of electrons in the solar wind at energies $20 \lesssim E \lesssim 10^3$ eV (ref. 52 and sec. 2.1.3.3). In these crude approximations the heliocentric distance S is in AU and the electron kinetic energy E is in MeV for $2 \times 10^{-5} < E < 10$ MeV. At higher energies galactic cosmic ray electrons dominate (sec. 2.2).

3. CRITERIA

Quantitative descriptions for charged particle environments in interplanetary space that include time, position and energy dependences, probabilities, and other parameters are recommended for design and mission planning in the following sections. The environments consist of solar wind, energetic solar protons and electrons, and galactic cosmic rays. The descriptions apply everywhere in interplanetary space between 0.1 and 10 AU from the Sun except within the magnetospheres of the Earth and other planets with magnetic fields.

Within the magnetospheres, the planetary magnetic fields exclude the solar wind but permit entry of solar particles and galactic cosmic rays; these are less concentrated at lower Earth altitudes than in interplanetary space. Their intensities are enhanced by trapped radiation belts and magnetospheric plasma. The trapped radiation belts of the Earth are described in NASA SP-8116, the trapped radiation belts of Jupiter in SP-8069, the belts of Saturn in SP-8091, and the belts of Uranus and Neptune in SP-8103.

For this monograph, table 1 gives the sections in which intensities are found for the particle kinds and energy ranges of interplanetary space. Basic relationships between intensity, flux, and fluence can be obtained from the definitions of symbols and terms in appendices A and B.

TABLE 1
INTERPLANETARY CHARGED PARTICLE INDEX

PARTICLE	CHARGE AND MASS	ENERGY RANGE	SECTION
Protons	$e = 1.602 \times 10^{-19} \text{ C}$ $m_p = 1.67 \times 10^{-27} \text{ kg}$	$\lesssim 1 \text{ keV}$ (Solar Wind)	3.1 (table 2)
		1 keV to 10 MeV	3.3.3
		10 to 10^3 MeV (Solar Particle Events)	3.3.1 and 3.3.2
		$>10 \text{ MeV}$ (Galactic Cosmic Rays)	3.2
Other Ions and Nuclei	$+Ze$ Am_p	$\lesssim 10^{-3} \text{ MeV}$ (Solar Wind)	3.1
		10^{-3} to 10 MeV/nucleon	3.3.3
		$>10 \text{ MeV/nucleon}$ (Galactic Cosmic Rays)	3.2 (table 3)
Electrons	$-e$ $m_e = 9.11 \times 10^{-31} \text{ kg}$	$\lesssim 20 \text{ eV}$ (Solar Wind)	3.1 (table 2)
		20 eV to 10 MeV	3.3.3
		$>10 \text{ MeV}$ (Galactic Cosmic Rays)	3.2
Positrons	$+e$ m_e	$>1 \text{ MeV}$ (Galactic Cosmic Rays)	3.2

3.1 Solar Wind

The solar wind is fully-ionized plasma continuously streaming approximately outward from the Sun with variable concentrations, velocities, and temperatures of electrons, protons, and heavier positive ions, and with entraining magnetic field lines. Table 2 specifies average values, ranges, and dependences on heliocentric distance S ; the median, average, and most probable values are comparable. The range of observed instantaneous values (any time scale \lesssim a week) is somewhat broader than the range given in table 2; at different times, extreme concentrations up to 200 cm^{-3} , speeds up to 1000 km/s, and magnetic field strengths up to 30 nT (30 gamma) have been observed near the Earth. Commonly streams of solar wind plasma exist, with high flow speed and temperature associated with low concentrations; interactions within and among moving streams include acoustic and plasma waves, shocks,

and discontinuities. To estimate cumulative (any time scale \geq a month) effects of solar wind impact, average values are appropriate. For heavier ions in the solar wind, both the flow and thermal speeds match those of the protons; their concentrations are $\lesssim (0.2 \text{ cm}^{-3})S^{-2}$, a typical value for He^{++} (the most common ion after H^+).

TABLE 2
VALUES NEAR 1 AU AND RADIAL DEPENDENCES
FOR SOLAR WIND PARAMETERS

PARAMETER	AVERAGE	RANGE*	RADIAL DEPENDENCE
Protons			
concentration, cm^{-3}	5	7 to 2.5	S^{-2}
flow speed, km/s	425	350 to 550	none
thermal speed, km/s	50	35 to 70	$S^{-0.5}$
temperature, K	8×10^4	(5 to 15) $\times 10^4$	$S^{-1 \pm 0.5}$
energy (flow), eV	900	600 to 1500	none
flux (flow), $\text{m}^{-2}\text{s}^{-1}$	2×10^{12}	(2.5 to 1.4) $\times 10^{12}$	S^{-2}
pressure, N/m^2	1.5×10^{-9}	(1.6 to 1.2) $\times 10^{-9}$	S^{-2}
Electrons			
concentration, cm^{-3}	5	7 to 2.5	S^{-2}
flow speed, km/s	425	<u>350 to 550</u> **	none
thermal speed, km/s	2700	2100 to 3300	$S^{-0.5}$
temperature, K	1.5×10^5	(1 to 2) $\times 10^5$	$S^{-1 \pm 0.5}$
energy (thermal), eV	20	13 to 30	$S^{-1 \pm 0.5}$
flux (thermal) $\text{m}^{-2}\text{s}^{-1}$	10^{13}	(5 to 15) $\times 10^{12}$	$S^{-2.5 \pm 0.25}$
Magnetic Field			
strength, nT (gammas)	5	2 to 8	S^{-1}

*Typically data fall within this range about 60% of the time; some extremes are cited in section 3.1. For surfaces shielded from the flow, e.g., in a spacecraft's wake, electron properties are unchanged but protons are absent.

**Stream correlated quantities appear above the dashed line with fast stream values at right and slow at left; below the line parameters are not strongly correlated with streams.

3.2 Galactic Cosmic Rays

Galactic cosmic rays are relativistic charged particles (predominantly protons, with some electrons, positrons, and heavy nuclei) continuously present in interplanetary space at

integral fluxes $\gtrsim 3 \times 10^4 \text{ m}^{-2} \text{ s}^{-1}$ and energies extending indefinitely upward from below 100 MeV. In the following equations, the cosmic ray intensities are considered independent of time, direction, and location in interplanetary space with the exception of the time variations of E_2 (eqs. 16 through 18). The numerical representations (eqs. 14 through 17) for the integral and differential intensities are diagrammed in figure 14.

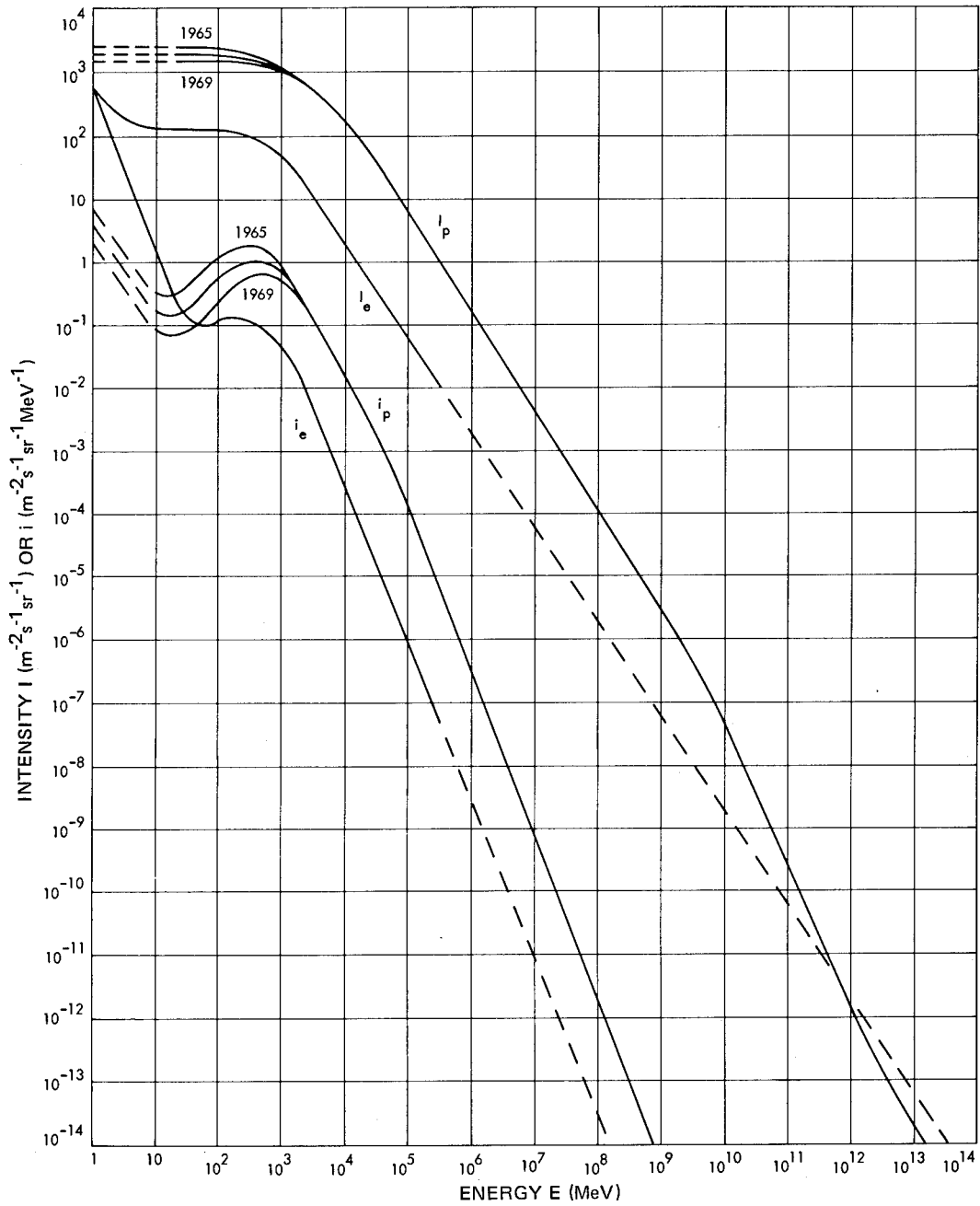


Figure 14.—Intensity spectra of galactic cosmic ray electrons and protons. Solid portions represent data and dashed portions extrapolations. The three branches of the proton curves represent solar cycle modulation in 1965, 1967, and 1969.

3.2.1 Electron Component

The electron curves in figure 14 for the mean integral and differential intensities versus kinetic energy are specified by

$$I_e = \frac{2000}{(\alpha E^6 + \beta E^3 + E^2 + \gamma)^{1/4}} + \frac{400}{E^{3/2}} \quad (14)$$

and

$$i_e = \frac{500(6\alpha E^5 + 3\beta E^2 + 2E)}{(\alpha E^6 + \beta E^3 + E^2 + \gamma)^{5/4}} + \frac{600}{E^{5/2}} \quad (15)$$

Here the required units are E in MeV (for $1 < E < 3 \times 10^5$ MeV), I_e in $m^{-2} s^{-1} sr^{-1}$, and i_e in $m^{-2} s^{-1} sr^{-1} MeV^{-1}$; and the parameter values are $\alpha = 10^{-12}$, $\beta = 10^{-3}$, and $\gamma = 6 \times 10^4$. For a precision within 1%, terms proportional to α may be ignored for $E < 250$ MeV and the last of the terms in the sum for I_e or i_e may be ignored for $E > 250$ MeV. The data on which the electron representations are based have a scatter of less than 25% about the curves. The positron intensities are $0.1 \times 2^{z-1}$ times the electron intensities (eqs. 14 and 15) at the same energy.

3.2.2 Proton Component

The proton curves in figure 14 for the mean integral and differential intensities versus kinetic energy are specified by

$$I_p = \frac{3 \times 10^5}{[\alpha E^6 + \beta E^4 + E^2 + (1.8)E_2^2]^{2/5}} + \frac{10^7}{E^{3/5}(E + \gamma E_2^2)} \quad (16)$$

and

$$i_p = \frac{1.2 \times 10^5 (6\alpha E^5 + 4\beta E^3 + 2E)}{[\alpha E^6 + \beta E^4 + E^2 + (1.8)E_2^2]^{7/5}} + \frac{10^7 [(1.6)E + 0.6\gamma E_2^2]}{E^{8/5}(E + \gamma E_2^2)^2} \quad (17)$$

Here the required units are the same as for electrons, and the parameter values are $\alpha = 9 \times 10^{-29}$, $\beta = 5 \times 10^{-9}$, and $\gamma = 8$. For a precision within 1%, terms proportional to α may be ignored for $E < 10^9$ MeV, terms proportional to β may be ignored for $E < 2000$ MeV, and the last of the two terms in the sum for I_p or i_p may be ignored for $80 < E < 10^{10}$ MeV. The energy parameter E_2 represents the location of a maximum in the proton differential intensity i_p and is variable in the solar cycle. Suitable values are shown in figure 13 and are given by

$$E_2 = \begin{cases} 576 - 164(t - 1970) & \text{for } 1964.75 \leq t \leq 1975.25 \\ 576 - 164(t - 1980.5) & \text{for } 1975.25 \leq t \leq 1985.75 \end{cases} \quad (18)$$

where t represents the date in solar cycle 20 or 21. The data on which the proton representations are based have a scatter of less than 50% about the curves.

3.2.3 Other Nuclei

For the same values of kinetic energy E , specified in MeV/nucleon, the intensities of other cosmic ray nuclei are related to the proton intensities (eqs. 16 and 17) by the factors specified in table 3.

TABLE 3
INTENSITY RATIOS OF THE TWELVE MOST ABUNDANT
COSMIC RAY NUCLEI TO PROTONS

NUCLEUS	ATOMIC NUMBER (CHARGE)	ATOMIC WEIGHT (NUCLEONS)	RATIO TO PROTONS*
H	1	1	1.0
He	2	4	0.1
Li	3	7	4×10^{-4}
Be	4	9	2.5×10^{-4}
B	5	11	6×10^{-4}
C	6	12	2.5×10^{-3}
N	7	14	6×10^{-4}
O	8	16	2.5×10^{-3}
Ne	10	20	4×10^{-4}
Mg	12	24	4×10^{-4}
Si	14	28	3×10^{-4}
Fe	26	56	2.5×10^{-4}

*Accuracy in most cases better than 50%.

3.3 Solar Particle Events

Solar particle events are sporadic injections of energetic charged particles from the Sun into interplanetary space at very irregular intervals that are related to solar activity. Within each event, the particle intensity varies markedly with time (from time scales of less than a second to a few days for the rise and decay of an entire event), position, direction, and energy. These intensity variations are unpredictable for any given combinations of individual event and detector trajectory so in the following description only the peak intensity (independent of time, position, and direction) and cumulative event fluence are specified on a probabilistic basis for a range of particle energies.

The following two sections describe a technique which permits for an interplanetary mission of time interval $t_1 < t < t_2$, the derivation of the intensity I and fluence F that will be exceeded with a probability P . The analysis has two branches from which one can be

selected on the basis of whether ordinary (OR) or anomalously large (AL) events dominate for a particular mission and probability.

3.3.1 Peak Proton Intensity

To include the relative event frequencies during the active and inactive portions of the solar cycle, compute the reduced time interval τ where

$$\tau = \int_{t_1}^{t_2} f(t) dt \quad (19)$$

where the weighting function $f(t)$ takes the value 1.0 during the seven most active years of each solar cycle (1977 through 1983 for cycle 21) and 0.3 at all other times. To include the relative severity of events observed at variable heliocentric distances $S \neq 1$ AU, compute the weighting factor

$$W_m = \frac{1}{(t_2 - t_1)} \int_{t_1}^{t_2} [S(t)]^{-m} f(t) dt. \quad (20)$$

For the computation of mission peak intensity I , the following procedures should be used. With τ from equation 19 and the probability P (sec. 3.3), figure 11 is used to determine whether AL events or OR events alone should be considered, according to the side of line $N = 1$ on which point (τ, P) falls. Should it fall below and to the right of the $N = 1$ line, the appropriate AL event intensities at $S = 1$ AU are given for four energy thresholds in the top half of table 4. Should the point (τ, P) fall above and to the left of the $N = 1$ line, the appropriate OR event intensity at $S = 1$ AU can be read from figure 9 and scaled to energy thresholds ($\neq 30$ MeV) by application of the OR event peak intensities specified by $(\log D)$ in table 4. In either case, the intensity should also be multiplied by the weighting factor W_3 computed from equation 20, using $m = 3$.

3.3.2 Proton Fluence

Just as for the peak proton intensity, τ , P , and figure 11 are used to determine whether AL or OR events dominate the case of interest. If the AL events dominate, the corresponding number of AL events can be interpolated from figure 12 and multiplied by the single AL event fluence entries in table 4. If the OR events dominate, the fluence for $E_p > 30$ MeV can be read from figure 10 and scaled to other energies using the $(\log F)$ entries for OR events in table 4. In either case the fluence should be multiplied by the weighting factor W_2 computed from equation 20, using $m = 2$.

3.3.3 Other Particles and Energies

The foregoing proton description serves in the energy range $10 \leq E \leq 100$ MeV, and provisionally up to 1000 MeV as well. Near the latter energy, very rare proton events (not more than about two per cycle) can reach brief (hours or less) peak integral intensities near

$$I = (4 \times 10^6 \text{ m}^{-2} \text{ s}^{-1} \text{ sr}^{-1})(E/1000 \text{ MeV})^{-2} \text{ S}^{-3}$$

TABLE 4
PARAMETERS FOR AL EVENT (AUGUST, 1972) AND FOR LOG-NORMAL PROTON
DISTRIBUTIONS REPRESENTING OR EVENTS (Cycle 20)

TYPE OF EVENT	PARAMETERS	$E_p > 10 \text{ MeV}$	$E_p > 30 \text{ MeV}$	$E_p > 60 \text{ MeV}$	$E_p > 100 \text{ MeV}$
AL EVENTS	Peak Intensity, I ($\text{m}^{-2}\text{s}^{-1}\text{sr}^{-1}$)	8.8×10^8	2.1×10^8	6.4×10^7	3×10^7
	Fluence, F (m^{-2})	2.25×10^{14}	8.1×10^{13}	2.45×10^{13}	5.5×10^{12}
OR EVENTS	Peak Intensity, $\langle \log I \rangle \pm \sigma_I$ ($\text{m}^{-2}\text{s}^{-1}\text{sr}^{-1}$)	6.61 ± 0.41	5.81 ± 0.60	5.32 ± 0.53	(5.0 ± 0.5)
	Fluence, $\langle \log F \rangle \pm \sigma_F$ (m^{-2})	12.81 ± 0.29	11.92 ± 0.45	11.41 ± 0.44	10.78 ± 0.47

where $\gamma = 0.7$ for $E < 1000 \text{ MeV}$ and $\gamma = 4$ for $E > 1000 \text{ MeV}$ (for details consult T. Foelsche in NASA TMX-2440, 1972, pp. 894-901 and in NASA SP-71, SP-169, and NASA-TND-7715). Except for such events, galactic cosmic ray protons (sec. 3.2) dominate above 1000 MeV.

In the interval between solar wind energies (1 KeV and 10 MeV), expressions that approximate the peak solar proton integral intensity in the form $I = (10^8 \text{ m}^{-2} \text{ s}^{-1} \text{ sr}^{-1})/S^3 E^{1.2}$ and the average solar proton integral intensity $I = (10^6 \text{ m}^{-2} \text{ s}^{-1} \text{ sr}^{-1})/S^2 E^{1.7}$ are appropriate for heliocentric distance S in AU and proton kinetic energy E in MeV for $10^{-3} < E < 10 \text{ MeV}$. Fluence can be derived from the average integral intensity. At all energies, helium nuclei intensities are of the order of 0.05 times the proton intensities but may range from 0.0 to 0.25. Other positive ions may be neglected.

For solar particle event electrons, expressions that approximate the peak electron integral intensity $I = (10^5 \text{ m}^{-2} \text{ s}^{-1} \text{ sr}^{-1})/S^3 E^2$ and the average electron integral intensity $I = (400 \text{ m}^{-2} \text{ s}^{-1} \text{ sr}^{-1})/S^2 E^2$ are appropriate for heliocentric distance S in AU and electron kinetic energy E in MeV for $2 \times 10^{-5} < E < 10 \text{ MeV}$. Fluence can be derived from the average integral intensity. Beyond this energy range the solar wind or galactic cosmic ray electron descriptions apply.

REFERENCES

1. Parker, E. N.: Dynamics of the Interplanetary Gas and Magnetic Fields. *Astrophysical Journal*, Vol. 123, 1958, pp. 664-675.
2. Brandt, J. C.: *Introduction to the Solar Wind*. Freeman, San Francisco, 1970, 199 pp.
3. Bhatnagar, V. P. and Fahr, H. J.: Solar Wind Expansion Beyond the Heliosphere. *Planetary Space Science*, Vol. 20, No. 4, 1972, pp. 445-460.
4. Axford, W. I.: Interaction of the Solar Wind with the Interstellar Medium. NASA SP-308, 1972, pp. 609-660.
5. Brandt, J. C.: Interplanetary Gas XIII. Gross Plasma Velocities from the Orientations of Ionic Comet Tails. *Astrophysical Journal*, Vol 147, No. 1, 1967, pp. 201-219.
6. Axford, W. I.: Observations of the Interplanetary Plasma. *Space Science Reviews*, Vol. 8, No. 3, 1968, pp. 331-365.
7. Cohen, M. H.; Gundermann, E. J.; Hardebeck, H. E.; and Sharp, L. E.: Interplanetary Scintillations II. Observations. *Astrophysical Journal*, Vol. 147, No. 2, 1967, pp. 449-466.
8. Hewish, A. and Symonds, M. D.: Radio Investigation of the Solar Plasma. *Planetary Space Science*, Vol. 17, 1969, pp. 313-320.
9. Hundhausen, A. J.; Bame, S. J.; Asbridge, J. R.; and Sydoriak, S. J.: Solar Wind Proton Properties: Vela 3 Observations from July 1965 to June 1967. *Journal of Geophysical Research*, Vol. 75, No. 25, 1970, pp. 4643-4657.
10. Wolfe, J. H.: Large Scale Structure of the Solar Wind. NASA SP-308, 1972, pp. 170-201.
11. Bame, S. J.; Asbridge, J. R.; Hundhausen, A. J.; and Montgomery, M. D.: Solar Wind Ions: $^{56}\text{Fe}^{+8}$ to $^{56}\text{Fe}^{+12}$, $^{28}\text{Si}^{+7}$, $^{28}\text{Si}^{+8}$, $^{28}\text{Si}^{+9}$, and $^{16}\text{O}^{+6}$. *Journal of Geophysical Research*, Vol. 75, No. 31, 1970, pp. 6360-6365.
12. Bame, S. J.: Spacecraft Observations of the Solar Wind Composition. NASA SP-308, 1972, pp. 535-558.
13. Montgomery, M. D.: Average Thermal Characteristics of Solar Wind Electrons. NASA SP-308, 1972, pp. 208-218.
14. Ness, N. F.; Hundhausen, A. J.; and Bame, S. J.: Observations of the Interplanetary Medium: Vela 3 and IMP 3, 1965-1967. *Journal of Geophysical Research*, Vol. 76, No. 28, 1971, pp. 6643-6660.

15. Davis, L., Jr.: The Interplanetary Magnetic Field. NASA SP-308, 1972, pp. 93-114.
16. Burlaga, L. F.: Microstructure of the Interplanetary Medium. NASA SP-308, 1972, pp. 309-332.
17. Neugebauer, M. and Snyder, C. W.: Mariner 2 Observations of the Solar Wind, 1. Average Properties. *Journal of Geophysical Research*, Vol. 71, No. 19, 1966, pp. 4469-4484.
18. Cupperman, S.; Harten, A.; and Dryer, M.: Characteristics of the Quiet Solar Wind Beyond the Earth's Orbit. *Astrophysical Journal*, Vol. 177, No. 2, 1972, pp. 555-566.
19. Sreenkantan, B. V.: Primaries of Extensive Air Showers of Cosmic Radiation. *Space Science Reviews*, Vol. 14, No. 1, 1972, pp. 103-174.
20. Hsieh, K. C.; Mason, G. M. and Simpson, J. A.: Cosmic-Ray ^2H from Satellite Measurements, 1965-1969. *Astrophysical Journal*, Vol. 166, No. 1, 1971, pp. 221-233.
21. Simpson, J. A.: Galactic Sources and the Propagation of Cosmic Rays. Paper presented at the 12th International Conference on Cosmic Rays, Hobart, Tasmania, 1971.
22. Webber, W. R.; Damle, S. V.; and Kish, J.: Studies of the Chemical Composition of Cosmic Rays with $Z = 3 - 30$ at High and Low Energies. *Astrophysics and Space Science*, Vol. 15, No. 2, 1972, pp. 245-271.
23. McDonald, F. B.; Cline, T. L.; and Simnett, G. M.: Multifarious Temporal Variations of Low-Energy Relativistic Cosmic-Ray Electrons. *Journal of Geophysical Research*, Vol. 77, No. 13, 1972, pp. 2213-2231.
24. Fichtel, C. E. and Reames, D. V.: Cosmic-Ray Propagation. *Physical Review*, Vol. 175, No. 5, 1968, pp. 1564-1576.
25. Jokipii, J. R.: Propagation of Cosmic Rays in the Solar Wind. *Reviews of Geophysics and Space Physics*, Vol. 9, No. 1, 1971, pp. 27-87.
26. O'Gallagher, J. J.: Observations of the Radial Gradient of Galactic Cosmic Radiation over a Solar Cycle. *Reviews of Geophysics and Space Physics*, Vol. 10, No. 3, 1972, pp. 821-835.
27. Webber, W. R. and Lezniak, J. A.: Interplanetary Radial Gradients of Galactic Cosmic Ray Protons and Helium Nuclei: Pioneer 8 and 9 Measurements from 0.75 to 1.10 AU. *Journal of Geophysical Research*, Vol. 78, No. 13, 1973, pp. 1979-2000.
28. Van Allen, J. A.: Heliocentric Radial Dependence of Galactic Cosmic Ray Intensity to and Beyond 3.0 A.U. *AGU Transactions EOS*, Vol. 54, No. 4, 1973, p. 407.

29. Urch, I. H. and Gleeson, L. J.: Radial Gradients and Anisotropies due to Galactic Cosmic Rays. *Astrophysics and Space Sciences*, Vol. 16, No. 1, 1972, pp. 55-74.
30. Earl, J. A.: Modulation of Cosmic-Ray Electrons. *Astrophysical Journal*, Vol. 178, No. 3, 1972, pp. 857-862.
31. Schmidt, P. J.: Cosmic-Ray Electron Spectrum and Its Modulation near Solar Maximum. *Journal of Geophysical Research*, Vol. 77, No. 19, 1972, pp. 3295-3310.
32. McDonald, F. B.: *Solar Proton Manual*. NASA TR R-169, 1963, 117 pp.
33. McCracken, K. C.; Rao, U. R.; and Ness, N. F.: Interrelationship of Cosmic-Ray Anisotropies and the Interplanetary Magnetic Field. *Journal of Geophysical Research*, Vol. 73, No. 13, 1968, pp. 4159-4166.
34. Engle, R. C.: A Computational Model for Solar Flare Particle Propagation. *Journal of Geophysical Research*, Vol. 76, No. 4, 1971, pp. 768-791.
35. Webb, S. and Quenby, J. J.: Numerical Studies of the Transport of Solar Protons in Interplanetary Space. *Planetary Space Science*, Vol. 21, No. 1, 1973, pp. 23-42.
36. Thomas, J. R.: Mariner Venus-Mercury 1973 Mission Solar Proton Environment: Fluence and Dose. *JPL Quarterly Technical Review*, Vol. 2, No. 1, 1972, pp. 12-28.
37. Haffner, J. W.: Time Behavior of Solar Flare Particles to 5 AU. NASA TM X-2440, 1972, pp. 336-344.
38. Weddell, J. B. and Haffner, J. W.: Statistical Evaluation of Proton Radiation from Solar Flares. Report SID 66-421, North American Aviation, Downey, 1966, 178 pp.
39. Webber, W. R.: An Evaluation of the Radiation Hazard due to Solar Particle Events. Report D2-90469, Boeing, Seattle, 1963, 109 pp.
40. Atwell, W.: The Significant Solar Proton Events in the 20th Solar Cycle for the Period October 1964 to March 1970. NASA TM X-2440, 1972, pp. 329-335.
41. Yucker, W. B.: Solar Cosmic Ray Hazard to Interplanetary and Earth-Orbital Space Travel. NASA TM X-2440, 1972, pp. 345-355.
42. King, J. H.: Solar Proton Fluences for 1977-1983 Space Missions. *Journal of Spacecraft Rockets*, Vol. 11, No. 6, 1974, pp. 401-408.
43. Gonzalez, C. C. and Divita, E. L.: Solar Proton Forecast System and Procedures Used During the Mariner V Mission. JPL TR 32-1303, 1968, 35 pp.
44. Burrell, M. O.: The Risk of Solar Proton Events to Space Missions. NASA TM X-2440, 1972, pp. 310-323.

45. Dollman, T. S. and Bechtelheimer, A. T.: Construction of Probability Envelopes of Flux-Energy Spectrum for Solar Proton Events. NASA TM X-53647, 1967, pp. 110-113.
46. Roberts, W. T.: Probabilities of Solar Flare Occurrence. NASA TM X-53463, 1966, 12 pp.
47. Wilson, J. W.: Solar Radiation Hazard for Mars Orbiter. Private communication, 1971.
48. Frank, L. A.: On the Presence of Low-Energy Protons ($5 \lesssim E \lesssim 20$ keV) in the Interplanetary Medium. Journal of Geophysical Research, Vol. 75, No. 4, 1970, pp. 707-716.
49. Dietrich, W. F.: The Differential Energy Spectra of Solar-Flare ^1H , ^3He , and ^4He . Astrophysical Journal, Vol. 180, No. 3, 1973, pp. 955-973.
50. Cline, T. L. and McDonald, F. B.: Relativistic Electrons from Solar Flares. Solar Physics, Vol. 5, No. 4, 1968, pp. 507-530.
51. Lin, R. P. and Anderson, K. A.: Electrons > 40 keV and Protons > 500 keV of Solar Origin. Solar Physics, Vol. 1, No. 3/4, 1967, pp. 446-464.
52. Montgomery, M. D.; Bame, S. J.; and Hundhausen, A. J.: Solar Wind Electrons: Vela 4 Measurements. Journal of Geophysical Research, Vol. 73, No. 15, 1968, pp. 4999-5003.

APPENDIX A

SYMBOLS*

A	anisotropy, or atomic mass number
B	magnetic field strength (nT)
c	speed of light (3×10^8 m/s)
d Ω	infinitesimal solid angle (sr)
e	elementary charge (1.602×10^{-19} C)
E	charged particle kinetic energy (MeV)
E ₂	energy parameter for galactic cosmic ray protons (MeV)
f	differential fluence ($\text{m}^{-2}\text{MeV}^{-1}$)
F	integral fluence (m^{-2})
i	differential intensity ($\text{m}^{-2}\text{s}^{-1}\text{sr}^{-1}\text{MeV}^{-1}$)
I	integral intensity ($\text{m}^{-2}\text{s}^{-1}\text{sr}^{-1}$)
j	differential (omnidirectional) flux ($\text{m}^{-2}\text{s}^{-1}\text{MeV}^{-1}$)
J	integral (omnidirectional) flux ($\text{m}^{-2}\text{s}^{-1}$)
m _e	electron rest mass (9.11×10^{-31} kg)
m _p	proton rest mass (1.67×10^{-27} kg)
N	number of observed solar proton events
n	predicted number of solar proton events
p	charged particle momentum (kg m/s)
p(x)	probability density for solar proton log I, peak intensity
q(y)	probability density for solar proton log F, event fluence
R	rigidity (MV)
R _z	monthly smoothed Zürich sunspot number
S	heliocentric distance (AU)
t	time (calendar years)
T	past time interval (yr), for observed solar proton events

*Words in bold face are defined in Glossary (appendix B).

- W_m weighting function for solar proton I or F
 Z atomic charge number
 $\left. \begin{matrix} a \\ \beta \end{matrix} \right\}$ parameters in numerical representations of galactic cosmic ray **intensity**
 γ parameter in numerical representations of galactic cosmic ray and solar high energy proton **intensities**
 σ_I, σ_F parameters of distributions of solar proton peak **intensity, fluence**
 τ future time interval (yr), for solar proton event predictions

APPENDIX B

GLOSSARY*

Anisotropy (A) – The anisotropy is a dimensionless measure of the sensitivity of the local particle distribution (or intensity) to direction (of incidence). There are diverse formal definitions, in all of which $A = 0$ when the distribution is isotropic (independent of direction); otherwise, for $A > 0$, sample usage includes $A = (I_{\text{max}} - I_{\text{min}})/I_{\text{max}}$ where I_{max} and I_{min} are intensities in the directions of maximum and minimum intensity, or $A = (T_{\perp} - T_{\parallel})/T_{\parallel}$ where T_{\perp} and T_{\parallel} are temperatures perpendicular and parallel to the local magnetic field.

Fluence (f or F) – The fluence is the number of particles entering a unit area in a finite time. Like intensity (the basic quantity), it is differential (f) or integral (F). Thus $f = \int j \, dt = \int \int i \, d\Omega \, dt = -dF/dE$ and $F = \int j \, dt = \int_{E_1}^{\infty} dE \int \int i \, d\Omega \, dt = \int_{E_1}^{\infty} f \, dE$. Units for f are $\text{m}^{-2} \text{MeV}^{-1}$ and for F are m^{-2} .

Flux (j or J) – The omnidirectional flux is the number of particles entering a unit area per unit time. Like intensity (the basic quantity), it is differential (j) or integral (J). Thus $j = \int i \, d\Omega = -dJ/dE$ and $J = \int i \, d\Omega = \int_{E_1}^{\infty} dE \int i \, d\Omega = \int_{E_1}^{\infty} j \, dE$. In the isotropic ($A = 0$) case, $j = 4\pi i$ and $J = 4\pi I$. Units for j are $\text{m}^{-2} \text{s}^{-1} \text{MeV}^{-1}$ and for J are $\text{m}^{-2} \text{s}^{-1}$.

Intensity (i or I) – The intensity is the number of particles crossing a unit area, per unit time, from within a unit solid angle. It may depend on direction as well as on time and position, and is either differential (i, per unit energy interval) or integral (I, for energies $> E$), in both cases depending on particle kinetic energy E. Thus $i = -dI/dE$ and $I = \int_{E_1}^{\infty} i \, dE$. Units for i are $\text{m}^{-2} \text{s}^{-1} \text{sr}^{-1} \text{MeV}^{-1}$ and for I are $\text{m}^{-2} \text{s}^{-1} \text{sr}^{-1}$.

Modulation – Modulation is the decrease in intensity of galactic cosmic ray energy spectra in interplanetary space compared to that in interstellar space. The variable decrease is greatest at low cosmic ray energies and during high solar activity (cf. figs. 6 and 14).

Rigidity (R) – The rigidity of a charged particle is the absolute value of pe/Zc , and the radius of curvature of its trajectory in a magnetic field is R/Bc . For relativistic particles of unit charge, R in MV approximately equals E in MeV, whereas for most nuclei ($A/Z \approx 2$), R in MV approximately equals $2E$ for E in MeV/nucleon.

*Cross references within the Glossary are indicated by bold face. Symbols are described in appendix A.

NASA SPACE VEHICLE DESIGN CRITERIA MONOGRAPHS

ENVIRONMENT

- SP-8005 Solar Electromagnetic Radiation, revised May 1971
- SP-8010 Models of Mars' Atmosphere (1974) revised December 1974
- SP-8011 Models of Venus Atmosphere (1972), revised September 1972
- SP-8013 Meteoroid Environment Model—1969 (Near Earth to Lunar Surface), March 1969
- SP-8017 Magnetic Fields—Earth and Extraterrestrial, March 1969
- SP-8020 Mars Surface Models (1968), May 1969
- SP-8021 Models of Earth's Atmosphere (90 to 2500 km), revised March 1973
- SP-8023 Lunar Surface Models, May 1969
- SP-8037 Assessment and Control of Spacecraft Magnetic Fields, September 1970
- SP-8038 Meteoroid Environment Model—1970 (Interplanetary and Planetary), October 1970
- SP-8049 The Earth's Ionosphere, March 1971
- SP-8067 Earth Albedo and Emitted Radiation, July 1971
- SP-8069 The Planet Jupiter (1970), December 1971
- SP-8084 Surface Atmospheric Extremes (Launch and Transportation Areas), revised June 1974
- SP-8085 The Planet Mercury (1971), March 1972
- SP-8091 The Planet Saturn (1970), June 1972
- SP-8092 Assessment and Control of Spacecraft Electromagnetic Interference, June 1972
- SP-8103 The Planets Uranus, Neptune, and Pluto (1971), November 1972

- SP-8105 Spacecraft Thermal Control, May 1973
- SP-8111 Assessment and Control of Electrostatic Charges, May 1974
- SP-8116 The Earth's Trapped Radiation Belts, March, 1975
- SP-8117 Gravity Fields of the Solar System, April 1975
- SP-8118 Interplanetary Charged Particle Models (1974), March 1975

STRUCTURES

- SP-9011 Buffeting During Atmospheric Ascent, revised November 1970
- SP-8002 Flight-Loads Measurements During Launch and Exit, revised June 1972
- SP-8003 Flutter, Buzz, and Divergence, July 1964
- SP-8004 Panel Flutter, revised June 1972
- SP-8006 Local Steady Aerodynamic Loads During Launch and Exit, May 1965
- SP-8007 Buckling of Thin-Walled Circular Cylinders, revised August 1968
- SP-8008 Prelaunch Ground Wind Loads, November 1965
- SP-8009 Propellant Slosh Loads, August 1968
- SP-8012 Natural Vibration Modal Analysis, September 1968
- SP-8014 Entry Thermal Protection, August 1968
- SP-8019 Buckling of Thin-Walled Truncated Cones, September 1968
- SP-8022 Staging Loads, February 1969
- SP-8029 Aerodynamic and Rocket-Exhaust Heating During Launch and Ascent, May 1969
- SP-8031 Slosh Suppression, May 1969
- SP-8032 Buckling of Thin-Walled Doubly Curved Shells, August 1969
- SP-8035 Wind Loads During Ascent, June 1970
- SP-8040 Fracture Control of Metallic Pressure Vessels, May 1970

SP-8042 Meteoroid Damage Assessment, May 1970

SP8043 Design-Development testing, May 1970

SP-8044 Qualification testing, May 1970

SP-8045 Acceptance testing, April 1970

SP-8046 Landing Impact Attenuation for Non-Surface-Planning Landers, April 1970

SP-8050 Structural Vibration Prediction, June 1970

SP-8053 Nuclear and Space Radiation Effects on Materials, June 1970

SP-8054 Space Radiation Protection, June 1970

SP-8055 Prevention of Coupled Structure-Propulsion Instability (Pogo), October 1970

SP-8056 Flight Separation Mechanisms, October 1970

SP-8057 Structural Design Criteria Applicable to a Space Shuttle, revised March 1972

SP-8060 Compartment Venting, November 1970

SP-8061 Interaction with Umblicals and Launch Stand, August 1970

SP-8062 Entry Gasdynamic Heating, January 1971

SP-8063 Lubrication, Friction, and Wear, June 1971

SP-8066 Deployable Aerodynamic Deceleration Systems, June 1971

SP-8068 Buckling Strength of Structural Plates, June 1971

SP-8072 Acoustic Loads Generated by the Propulsion System, June 1971

SP-8077 Transportation and Handling Loads, September 1971

SP-8079 Structural Interaction with Control Systems, November 1971

SP-8082 Stress-Corrosion Cracking in Metals, August 1971

SP-8083 Discontinuity in Metallic Pressure Vessels, November 1971

SP-8095 Preliminary Criteria for the Fracture Control of Space Shuttle Structures, June 1971

SP-8099 Combining Ascent Loads, May 1972

GUIDANCE AND CONTROL

SP-8015 Guidance and Navigation for Entry Vehicles, November 1968

SP-8016 Effects of Structural Flexibility on Spacecraft Control Systems, April 1969

SP-8018 Spacecraft Magnetic Torques, March 1969

SP-8024 Spacecraft Gravitational Torques, May 1969

SP-8026 Spacecraft Star Trackers, July 1970

SP-8027 Spacecraft Radiation Torques, October 1969

SP-8028 Entry Vehicle Control, November 1969

SP-8033 Spacecraft Earth Horizon Sensors, December 1969

SP-8034 Spacecraft Mass Expulsion Torques, December 1969

SP-8036 Effects of Structural Flexibility on Launch Vehicle Control Systems, February 1970

SP-8047 Spacecraft Sun Sensors, June 1970

SP-8058 Spacecraft Aerodynamic Torques, January 1971

SP-8059 Spacecraft Attitude Control During Thrusting Maneuvers, February 1971

SP-8065 Tubular Spacecraft Booms (Extendible, Reel Stored), February 1971

SP-8070 Spaceborne Digital Computer Systems, March 1971

SP-8071 Passive Gravity-Gradient Libration Dampers, February 1971

SP-8074 Spacecraft Solar Cell Arrays, May 1971

SP-8078 Spaceborne Electronic Imaging Systems, June 1971

SP-8086 Space Vehicle Displays Design Criteria, March 1972

SP-8096 Space Vehicle Gyroscope Sensor Applications, October 1972

SP-8098 **Effects of Structural Flexibility on Entry Vehicle Control Systems,**
June 1972

SP-8102 Space Vehicle Accelerometer Applications, December 1972

CHEMICAL PROPULSION

SP-8025 Solid Rocket Motor Metal Cases, April 1970

SP-8039 Solid Rocket Motor Performance Analysis and Prediction, May 1971

SP-8041 Captive-Fired Testing of Solid Rocket Motors, March 1971

SP-8048 Liquid Rocket Engine Turbopump Bearings, March 1971

SP-8051 Solid Rocket Motor Igniters, March 1971

SP-8052 Liquid Rocket Engine Turbopump Inducers, May 1971

SP-8064 Solid Propellant Selection and Characterization, June 1971

SP-8073 Solid Propellant Grain Structural Integrity Analysis, June 1973

SP-8075 Solid Propellant Processing Factors in Rocket Motor Design, October 1971

SP-8076 Solid Propellant Grain Design and Internal Ballistics, March 1972

SP-8080 Liquid Rocket Pressure Regulators, Relief Valves, Check Valves, Burst
Disks, and Explosive Valves, March 1973

SP-8081 Liquid Propellant Gas Generators, March 1972

SP-8087 Liquid Rocket Engine Fluid-Cooled Combustion Chambers, April 1972

SP-8088 Liquid Rocket Metal Tanks and Tank Components, May 1974

SP-8090 Liquid Rocket Actuators and Operators, May 1973

SP-8094 Liquid Rocket Valve Components, August 1973

SP-8097 Liquid Rocket Valve Assemblies, November 1973

SP-8100 Liquid Rocket Engine Turbopump Gears, March 1974

SP-8101 Liquid Rocket Engine Turbopump Shafts and Couplings, September 1972

SP-8110 Liquid Rocket Engine Turbines, January 1974